The Astronomical Journal, 132:781–800, 2006 August

A DATABASE OF 2MASS NEAR-INFRARED COLORS OF MAGELLANIC CLOUD STAR CLUSTERS

Peter M. Pessev, Paul Goudfrooij, Thomas H. Puzia, and Rupali Chandar[1]
Space Telescope Science Institute, 3700 San Martin Drive, Baltimore, MD 21218; pessev@stsci.edu, goudfroo@stsci.edu, tpuzia@stsci.edu, rupali@stsci.edu
Received 2005 December 9; accepted 2006 April 24

ABSTRACT

The (rest-frame) near-IR domain contains important stellar population diagnostics and is often used to estimate masses of galaxies at low, as well as high, redshifts. However, many stellar population models are still relatively poorly calibrated in this part of the spectrum. To allow an improvement of this calibration we present a new database of integrated near-IR JHK_s magnitudes for 75 star clusters in the Magellanic Clouds, using the Two Micron All Sky Survey (2MASS). The majority of the clusters in our sample have robust age and metallicity estimates from color-magnitude diagrams available in the literature, and populate a range of ages from 10 Myr to 15 Gyr and a range in [Fe/H] from −2.17 to +0.01 dex. A comparison with matched star clusters in the 2MASS Extended Source Catalog (XSC) reveals that the XSC only provides a good fit to the *unresolved* component of the cluster stellar population. We also compare our results with the often-cited single-channel *JHK* photometry of Persson and coworkers and find significant differences, especially for their 30″ diameter apertures, up to ∼2.5 mag in the *K* band, more than 1 mag in $J - K$, and up to 0.5 mag in $H - K$. Using simulations to center apertures based on maximum light throughput (as performed by Persson et al.), we show that these differences can be attributed to near-IR-bright cluster stars (e.g., carbon stars) located away from the true center of the star clusters. The wide age and metallicity coverage of our integrated JHK_s photometry sample constitute a fundamental data set for testing population synthesis model predictions and for direct comparison with near-IR observations of distant stellar populations.

Key words: galaxies: star clusters — galaxies: stellar content — infrared: general — infrared: stars — Magellanic Clouds — techniques: photometric

Online material: machine-readable tables

1. INTRODUCTION

Much of our understanding of galaxy formation and evolution comes from studying stellar populations in different galaxy types, in both the present and the early universe. Two key parameters of stellar systems that are widely used throughout the literature are mean ages and metallicities. Ages and/or metallicities of stellar systems in photometric surveys are estimated by comparing measured integrated colors with the predictions of evolutionary synthesis models (e.g., Bruzual & Charlot 1993, 2003; Worthey 1994; Vazdekis 1999; Maraston 1998, 2005). These models use stellar isochrone libraries, which are synthesized in appropriate combinations to represent stellar systems at different ages and metallicities. There are, however, two important limitations inherent to these models. First, the stellar libraries themselves contain mostly stars in the solar neighborhood, which have a star formation history that is not necessarily typical for extragalactic populations (e.g., relatively little variation in chemical composition). Second, the synthesis models oversimplify the more rapid (but very luminous) phases of stellar evolution (e.g., thermally pulsing asymptotic giant branch [AGB] stars). Given the very fundamental nature of the information that is derived by comparison with these models, it is imperative that population synthesis models be as accurate as possible.

Simple stellar population (SSP) models are empirically calibrated to observations of real star clusters for which ages and metallicities are known from independent analysis, e.g., color-magnitude diagrams (CMDs; e.g., Bruzual et al. 1997; Maraston et al. 2003). While much of the work to date has been carried out at optical wavelengths, the near-infrared (NIR) regime contains some very important diagnostics for deriving basic properties of stellar systems. In fact, this wavelength regime has been shown to be very important for sorting out the effects of age and metallicity, particularly in stellar populations older than about 300 Myr (e.g., Goudfrooij et al. 2001; Puzia et al. 2002; Hempel & Kissler-Patig 2004). Due to recent advances in the instrumentation and detector capabilities in the NIR passbands, and considering the focus on the infrared in the next generation of telescopes, it is clear that the accuracy of SSP models in the NIR is going to be even more important in the future.

In this work we present integrated NIR colors of a large sample of star clusters in the Large and Small Magellanic Clouds (LMC and SMC). We make use of data from the Two Micron All Sky Survey (2MASS; Skrutskie et al. 1997), which offers uniform, high-quality imaging of the entire sky in three bands, *J* (1.25 μm), *H* (1.65 μm), and K_s[2] (2.16 μm). Our main goal is to provide a new database of intrinsic NIR magnitudes and colors of clusters with well-known ages and metallicities from deep CMDs that can be used as a calibration data set for existing and future-generation SSP models. The clusters in the Magellanic Clouds are very suitable for addressing this issue. They cover a wide range of ages, and they are close enough for detailed CMD studies using the *Hubble Space Telescope* (in some cases also with large telescopes on the ground). Unlike the globular cluster system of our Galaxy, there are a significant number of objects with intermediate ages (0.3–3 Gyr) in the LMC and SMC. The integrated-light properties of these systems are affected strongly by AGB stars, which are extremely luminous in the NIR, and

[1] Current address: Department of Physics and Astronomy, Johns Hopkins University, 3400 North Charles Street, Baltimore, MD 21218.

[2] For a description of the "*K* short" (K_s) band, see Persson et al. (1998).

TABLE 1
SMC Cluster Sample

ID	$\alpha_{J2000.0}$[a]	$\delta_{J2000.0}$[a]	Age[b]	Ref.	[Fe/H]	Ref.	A_v[c]
NGC 121.....	00 26 49	−71 32 10	10.08 ± 0.05	8	-1.71 ± 0.10	8	0.18 ± 0.02
NGC 152.....	00 32 56	−73 06 59	$9.15^{+0.06}_{-0.07}$	3	-0.94 ± 0.15	3	0.19 ± 0.02
NGC 176.....	00 35 59	−73 09 57	8.30 ± 0.30	6, 7	−0.6	7	0.24 ± 0.03
NGC 330.....	00 56 20	−72 27 44	$7.40^{+0.20}_{-0.40}$	2, 4	-0.82 ± 0.11	5	0.37 ± 0.02
NGC 339.....	00 57 45	−74 28 21	$9.80^{+0.08}_{-0.10}$	8	-1.50 ± 0.14	8	0.18 ± 0.02
NGC 361.....	01 02 11	−71 36 25	$9.91^{+0.06}_{-0.07}$	8	-1.45 ± 0.11	8	0.17 ± 0.02
NGC 411.....	01 07 56	−71 46 09	$9.15^{+0.06}_{-0.07}$	1, 3	-0.68 ± 0.07	1, 3	0.17 ± 0.02
NGC 416.....	01 07 58	−72 21 25	$9.84^{+0.06}_{-0.08}$	8	-1.44 ± 0.12	8	0.20 ± 0.02
NGC 458.....	01 14 54	−71 32 58	$8.30^{+0.18}_{-0.30}$	4	-0.23 ± 0.25	4	0.23 ± 0.02
Kron 3.....	00 24 46	−72 47 37	$9.78^{+0.09}_{-0.11}$	8	-1.16 ± 0.09	8	0.18 ± 0.02
NGC 419.....	01 08 19	−72 53 03	9.08	9	−0.6	9	0.32 ± 0.02
Lindsay 1	00 04 00	−73 28 00	9.89	8	−1.35	8	0.18 ± 0.02
Lindsay 113	01 49 30	−73 43 00	9.60	8	−1.24	8	0.18 ± 0.02

[a] Positions are retrieved from the SIMBAD astronomical database. Units of right ascension are hours, minutes, and seconds, and units of declination are degrees, arcminutes, and arcseconds.
[b] The age for the clusters is given as log (age). The CMDs of the last three objects provide only a crude age estimation, and the errors are not given.
[c] The extinction information is retrieved from the Web site of the MCPS.
References.—(1) Alves & Sarajedini 1999; (2) Chiosi et al. 1995; (3) Crowl et al. 2001; (4) Da Costa & Hatzidimitriou 1998; (5) Hill 1999; (6) Hodge & Flower 1987; (7) Mackey & Gilmore 2003b; (8) Mighell et al. 1998; (9) Seggewiss & Richtler 1989.

their contribution to the light in that part of the spectrum is largely underestimated by most existing SSP models (see Maraston 2005).

The measurement of integrated magnitudes and colors of star clusters in the Magellanic Clouds is complicated by several factors. One problem is that of accurate centering of the aperture. Many of these clusters are superposed onto a relatively high surface density of stars associated with the LMC or SMC, and some have a rather irregular field distribution and/or are not particularly symmetric due to the superposition of bright stars (be it supergiants or AGB stars, associated with the cluster itself, those from the body of the LMC or SMC, or Galactic foreground stars). On the other hand, it should be recognized that the use of two-dimensional imagery renders these problems much less severe than they were for often-cited previous studies that used single-channel photometers and diaphragms that were centered either by eye or by maximum throughput.

The present study is complementary to the information about Magellanic Cloud clusters in the 2MASS Extended Source Catalog (XSC; Jarrett et al. 2000) in three ways: (1) providing photometry for a set of clusters that are not present in the 2MASS XSC, (2) taking into account the flux from the point sources associated with the star clusters, which are rejected by the XSC pipeline (see § 3.2 for details), and (3) better sampling of the curves of growth with a step of 1″, instead of 11 fixed circular apertures.

This paper is organized as follows: § 2 describes the sample selection, and data acquisition and reduction. The results, including comparison with previous works and the 2MASS XSC, are presented in § 3. Finally, a summary is provided in § 4.

2. NEAR-INFRARED DATA

2.1. *Sample Selection*

Our original sample of star clusters was adopted from Mackey & Gilmore (2003a, 2003b), and most have accurate CMD ages and metallicities from the literature. We particularly pay attention to the largest possible coverage of the available age/metallicity parameter space. In addition, we select intermediate-age and young clusters that have no known counterparts in the Milky Way globular cluster system. The adopted distance moduli are $m - M = 18.89$ and $m - M = 18.50$ for the SMC (Harries et al. 2003) and LMC (Alves 2004), respectively. Basic information for all objects is provided in Tables 1 and 2 (for star clusters in the SMC and LMC, respectively).

The young SMC cluster NGC 176 was included in the original list, but after inspection of the 2MASS images it became clear that the NIR data are too shallow to derive reliable integrated colors. R136 in LMC, the youngest object in the preliminary selection, is embedded in an extensive emission region that would affect the results of the integrated photometry. We decided not to include these two clusters in the final list. J, H, and K_s postage stamp images of representative objects in our sample are presented in Figures 1 (SMC) and 2 (LMC). V-band frames for the majority of the SMC objects included in this work can be found in Hill & Zaritsky (2006).

2.2. *2MASS Atlas Images*

The 2MASS Atlas Images originate from 6° long survey scans using an effective integration time of 7.8 s per tile. J, H, and K_s images were retrieved using the 2MASS interactive image service.[3] The queries were usually sent by object name and, in some cases when the name qualifier was not recognized, by coordinates. In most cases an object could be found on several sets of frames, allowing us to choose the best one, taking into account the relative position of the cluster and the characteristics of each field. Table 3 provides information on the atlas images selected for our study for the SMC and LMC clusters. The second column in the table provides the number of different sets of images retrieved for each object.

The raw survey data were reduced at the Infrared Processing and Analysis Center with the pipeline specifically developed for 2MASS. The imaging data are resampled to 1″ pixel^{-1}, are calibrated to 1 s integration time, and contain both the astrometric solution and the photometric zero points for each individual atlas image (Skrutskie et al. 2006). The astrometric solutions are obtained in the International Celestial Reference System via the Tycho-2 reference catalog. Taking into account the higher value of the extended source uncertainty (Skrutskie et al. 2006), all cluster positions derived in the present work were rounded to the nearest half pixel (0.″5).

[3] See http://irsa.ipac.caltech.edu/applications/2MASS/IM/interactive.html.

TABLE 2
LMC Cluster Sample

ID	$\alpha_{J2000.0}$[a]	$\delta_{J2000.0}$[a]	Age[b]	Ref.	[Fe/H]	Ref.	A_v^c
NGC 1466	03 44 33	−71 40 18	10.10 ± 0.01	8	−2.17 ± 0.20	16	0.39 ± 0.02
NGC 1651	04 37 32	−70 35 06	$9.30^{+0.08}_{-0.10}$	8	−0.37 ± 0.20	16	0.35 ± 0.05
NGC 1711	04 50 37	−69 59 06	7.70 ± 0.05	4	−0.57 ± 0.17	4	0.56 ± 0.01
NGC 1718	04 52 25	−67 03 06	9.30 ± 0.30	6	−0.42	13	0.51 ± 0.06
NGC 1754	04 54 17	−70 26 30	$10.19^{+0.06}_{-0.07}$	15	−1.54 ± 0.20	16	0.40 ± 0.04
NGC 1777	04 55 48	−74 17 00	$9.08^{+0.12}_{-0.18}$	8	−0.35 ± 0.20	16	0.39 ± 0.02
NGC 1786	04 59 06	−67 44 42	10.18 ± 0.01	8	−1.87 ± 0.20	16	0.62 ± 0.04
NGC 1805	05 02 21	−66 06 42	$7.00^{+0.30}_{-0.10}$	3	−0.25	3, 12	0.32 ± 0.02
NGC 1818	05 04 14	−66 26 06	$7.40^{+0.30}_{-0.10}$	3	−0.25	3, 12	0.39 ± 0.02
NGC 1831	05 06 16	−64 55 06	8.50 ± 0.30	6	+0.01 ± 0.20	16	0.39 ± 0.02
NGC 1835	05 05 05	−69 24 12	$10.22^{+0.07}_{-0.08}$	15	−1.79 ± 0.20	16	0.35 ± 0.07
NGC 1841	04 45 23	−83 59 48	10.09 ± 0.01	8	−2.11 ± 0.10	20	0.39 ± 0.02
NGC 1847	05 07 08	−68 58 18	7.42 ± 0.30	6	−0.37	13	0.49 ± 0.02
NGC 1850	05 08 44	−68 45 36	7.50 ± 0.20	5	−0.12 ± 0.20	11	0.33 ± 0.01
NGC 1856	05 09 29	−69 07 36	8.12 ± 0.30	6	−0.52	13	0.22 ± 0.03
NGC 1860	05 10 39	−68 45 12	8.28 ± 0.30	6	−0.52	13	0.27 ± 0.07
NGC 1866	05 13 39	−65 27 54	8.12 ± 0.30	6	−0.50 ± 0.10	9	0.28 ± 0.06
NGC 1868	05 14 36	−63 57 18	8.74 ± 0.30	6	−0.50 ± 0.20	16	0.39 ± 0.02
NGC 1898	05 16 42	−69 39 24	$10.15^{+0.06}_{-0.08}$	15	−1.37 ± 0.20	16	0.43 ± 0.05
NGC 1916	05 18 39	−69 24 24	10.20 ± 0.09	13	−2.08 ± 0.20	16	0.42 ± 0.05
NGC 1984	05 27 40	−69 08 06	7.06 ± 0.30	6	−0.90 ± 0.40	14	0.36 ± 0.02
NGC 2004	05 30 40	−67 17 12	7.30 ± 0.20	5	−0.56 ± 0.20	11	0.33 ± 0.02
NGC 2005	05 30 09	−69 45 06	$10.22^{+0.12}_{-0.16}$	15	−1.92 ± 0.20	16	0.47 ± 0.04
NGC 2011	05 32 19	−67 31 18	6.99 ± 0.30	6	−0.47 ± 0.40	14	0.47 ± 0.02
NGC 2019	05 31 56	−70 09 36	$10.25^{+0.07}_{-0.09}$	15	−1.81 ± 0.20	16	0.44 ± 0.06
NGC 2031	05 33 41	−70 59 12	8.20 ± 0.10	4	−0.52 ± 0.21	4	0.40 ± 0.03
NGC 2100	05 42 08	−69 12 42	7.20 ± 0.20	5	−0.32 ± 0.20	11	0.80 ± 0.02
NGC 2121	05 48 12	−71 28 48	$9.51^{+0.06}_{-0.07}$	17	−0.61 ± 0.20	16	0.53 ± 0.04
NGC 2136	05 53 17	−69 31 42	8.00 ± 0.10	4	−0.55 ± 0.23	4	0.58 ± 0.02
NGC 2153	05 57 51	−66 24 00	$9.11^{+0.12}_{-0.16}$	8	−0.42	13	0.27 ± 0.05
NGC 2155	05 58 33	−65 28 36	$9.51^{+0.06}_{-0.07}$	17	−0.55 ± 0.20	16	0.43 ± 0.04
NGC 2156	05 57 45	−68 27 36	7.60 ± 0.20	5	−0.45	13	0.20 ± 0.02
NGC 2157	05 57 34	−69 11 48	7.60 ± 0.20	5	−0.45	13	0.42 ± 0.02
NGC 2159	05 57 57	−68 37 24	7.60 ± 0.20	5	−0.45	13	0.29 ± 0.03
NGC 2162	06 00 31	−63 43 18	$9.11^{+0.12}_{-0.16}$	8	−0.23 ± 0.20	16	0.39 ± 0.02
NGC 2164	05 58 54	−68 31 06	7.70 ± 0.20	5	−0.45	13	0.33 ± 0.02
NGC 2172	06 00 05	−68 38 12	7.60 ± 0.20	5	−0.44	13	0.26 ± 0.03
NGC 2173	05 57 58	−72 58 42	$9.33^{+0.07}_{-0.09}$	8	−0.24 ± 0.20	16	0.39 ± 0.02
NGC 2193	06 06 17	−65 05 54	$9.34^{+0.09}_{-0.11}$	17	−0.60 ± 0.20	17	0.39 ± 0.02
NGC 2209	06 08 34	−73 50 30	$8.98^{+0.15}_{-0.24}$	8	−0.47	13	0.39 ± 0.02
NGC 2210	06 11 31	−69 07 18	10.20 ± 0.01	8	−1.97 ± 0.20	16	0.39 ± 0.02
NGC 2213	06 10 42	−71 31 42	$9.20^{+0.10}_{-0.12}$	8	−0.01 ± 0.20	16	0.40 ± 0.04
NGC 2214	06 12 57	−68 15 36	7.60 ± 0.20	5	−0.45	13	0.39 ± 0.02
NGC 2231	06 20 44	−67 31 06	$9.18^{+0.10}_{-0.13}$	8	−0.67 ± 0.20	16	0.39 ± 0.02
NGC 2249	06 25 49	−68 55 12	8.82 ± 0.30	6	−0.47	13	0.39 ± 0.02
NGC 2257	06 30 12	−64 19 36	10.20 ± 0.10	4	−1.63 ± 0.21	4	0.39 ± 0.02
SL 663	05 42 29	−65 21 48	$9.51^{+0.06}_{-0.07}$	17	−0.60 ± 0.20	17	0.38 ± 0.04
SL 842	06 08 15	−62 59 18	$9.30^{+0.08}_{-0.10}$	8	−0.36 ± 0.20	16	0.39 ± 0.02
SL 855	06 10 53	−65 02 36	9.13 ± 0.30	6	−0.42	13	0.39 ± 0.02
Hodge 4	05 31 54	−64 42 00	$9.34^{+0.09}_{-0.11}$	17	−0.15 ± 0.20	16	0.39 ± 0.02
Hodge 11	06 14 22	−69 50 54	10.18 ± 0.01	8	−2.06 ± 0.20	16	0.39 ± 0.02
Hodge 14	05 28 39	−73 37 48	$9.26^{+0.09}_{-0.11}$	8	−0.66 ± 0.20	16	0.39 ± 0.02
R136	05 38 43	−69 06 03	$6.48^{+0.12}_{-0.18}$	19	−0.40	10, 19	0.39 ± 0.02
ESO 121-003	06 03 24	−60 31 00	9.95	16, 18	−0.93	16, 18	0.39 ± 0.02
LW 431	06 13 27	−70 41 43	9.26	2	−0.85	2	0.39 ± 0.02
NGC 1751	04 54 12	−69 48 24	9.18	1	−0.18	1	0.65 ± 0.06
NGC 1783	04 59 08	−65 59 20	9.11	7	...	7	0.30 ± 0.03
NGC 1806	05 02 11	−67 59 20	8.70	1	−0.71	1	0.25 ± 0.04

TABLE 2—*Continued*

ID	$\alpha_{J2000.0}$[a]	$\delta_{J2000.0}$[a]	Age[b]	Ref.	[Fe/H]	Ref.	A_v[c]
NGC 1846	05 07 35	−67 27 39	9.46	1	−0.70	1	0.41 ± 0.04
NGC 1939	05 21 27	−69 56 59	10.04	1	−2.00	1	0.62 ± 0.05
NGC 1978	05 28 45	−66 14 12	9.32	7	−0.42	7	0.76 ± 0.05
NGC 1987	05 27 17	−70 44 06	9.40	1	−0.50	1	0.28 ± 0.03
NGC 2190	06 01 02	−74 43 30	9.04	1	−0.12	1	0.39 ± 0.02
NGC 2203	06 04 42	−75 26 20	9.26	7	−0.52	7	0.39 ± 0.02

[a] Positions are retrieved from the SIMBAD astronomical database. Units of right ascension are hours, minutes, and seconds, and units of declination are degrees, arcminutes, and arcseconds.

[b] The age for the clusters is given as log (age). The CMDs of the last 11 objects provide only a crude age estimation, and the errors are not given.

[c] The extinction information is retrieved from the Web site of the MCPS.

REFERENCES.—(1) Beasley et al. 2002; (2) Bica et al. 1998; (3) de Grijs et al. 2002; (4) Dirsch et al. 2000; (5) Elson 1991; (6) Elson & Fall 1988; (7) Geisler et al. 1997a; (8) Geisler et al. 1997b; (9) Hill et al. 2000; (10) Hunter et al. 1995; (11) Jasniewicz & Thevenin 1994; (12) Johnson et al. 2001; (13) Mackey & Gilmore 2003a; (14) Oliva & Origlia 1998; (15) Olsen et al. 1998; (16) Olszewski et al. 1991; (17) Rich et al. 2001; (18) Seggewiss & Richtler 1989; (19) Sirianni et al. 2000; (20) Suntzeff et al. 1992.

The photometric zero points are based on observations of fields, covering the NIR standards from the list of Persson et al. (1998) or the UKIRT group of faint equatorial NIR standard stars (Casali & Hawarden 1992). The solution is derived independently for each band and minimizes the residuals by a least-squares fit of the zero point, air mass, and atmospheric extinction (Nikolaev et al. 2000). The distributions of the zero-point differences for all standard fields in all survey nights turned out to be Gaussian, with rms residual values of 0.011, 0.007, and 0.007 mag in J, H, and K_s, respectively (Skrutskie et al. 2006). These values are added in quadrature to the photometric errors in this work.

2.3. *Data Analysis*

In order to measure the integrated cluster magnitudes, the following multistep procedure was applied to each object of the sample: (1) point-spread function (PSF)–fitting photometry of the point sources, (2) determination of the center position for the integrated curve of growth photometry, (3) subtraction of the background/foreground point source luminosity function (LF) from the LF of the cluster field, (4) integrated photometry of the total, background-subtracted, and unresolved component of the object in each survey band, and (5) calculation of the photometric errors for each measurement aperture.

For basic data analysis we use the suite of IRAF[4] tasks and perform DAOPHOT II ALLSTAR photometry (Stetson 1987) on each frame. Typically several bright and well-isolated stars are used to construct the PSF for each frame. As this is only an intermediate stage in the process of deriving the total integrated cluster magnitudes, aperture corrections are not applied at this point. The ALLSTAR routine is used to produce frames in which individual stars are removed after being measured. We refer to these frames as "residual frames," which will be used in a later paper to study the part of the cluster stellar population not resolved in the 2MASS images.

In many cases the coordinates taken from cluster catalogs in the literature do not provide an accurate position for the center of individual clusters. We applied a simple and robust method to derive the centers in the present paper. The original frames and the residual frames in each survey band were smoothed with a large Gaussian kernel. The size of the kernel varied as a function of the cluster size in the J frames, in which the sensitivity of 2MASS reaches its peak. The maximum flux values in an image subsection of the smoothed images in each of the survey bands, derived by the IRAF task *minmax*, were used to determine the individual cluster centers in J, H, and K_s. They were later averaged to derive the final center coordinates that were used for the integrated photometry in the present paper. Possible sources of confusion (e.g., bright stars outside the cluster area, present in the original atlas frames) were avoided by performing the procedure described earlier on an image subsection, covering the rough cluster position in the smoothed images. We point out that the cluster images in Figures 1 and 2 are extracted from the 2MASS frames, using the centers derived with this procedure. Each image covers $200'' \times 200''$ and is representative of the size of the largest aperture used to measure integrated cluster magnitudes.

In a few cases the object was situated close to the edge of the atlas frame. This was not a serious problem for most clusters because we were still able to sample the flux out to large enough radii to derive the total integrated magnitudes. One exception was Lindsay 1, which was split almost equally between two sets of frames. The special data reduction procedure applied to this object is described in § 2.7 below.

2.4. *Stellar Background Subtraction*

To estimate the contamination of our globular cluster fields by foreground stars and stars associated with the body of the LMC or SMC, we used the portion of the frames outside of the largest aperture used for integrated-light photometry (typical radius of $100''$). The LF for the point sources in these background regions was scaled to the cluster area used for photometry. This was statistically subtracted from the point-source LF obtained inside the photometric radius. The area of the background regions slightly varied as a function of the largest aperture size, but even in the case of $100''$ aperture radii it was more than 15 times larger than the photometry area. In this way we achieved a good estimate of the background/foreground contamination, one that is much less affected by local stellar variations and therefore superior to just subtracting a normalized background flux from a neighboring annulus. To illustrate our procedure, in Figure 3 we show the LFs of the background, cluster, and cleaned LF after the background subtraction for the heavily contaminated cluster NGC 330.

In cases in which bright stars (not sampled by the field star LF) were present in the cluster aperture, after the background subtraction we used their ALLSTAR PSF magnitudes and corresponding colors to make a rough estimation of the spectral and luminosity class using the work of Ducati et al. (2001). The visual magnitudes of these objects were recovered using the visual–infrared colors from the same study for a certain spectral and luminosity class.

[4] IRAF is distributed by the National Optical Astronomical Observatory, which is operated by the Associations of Universities for Research in Astronomy, Inc., under cooperative agreement with the National Science Foundation.

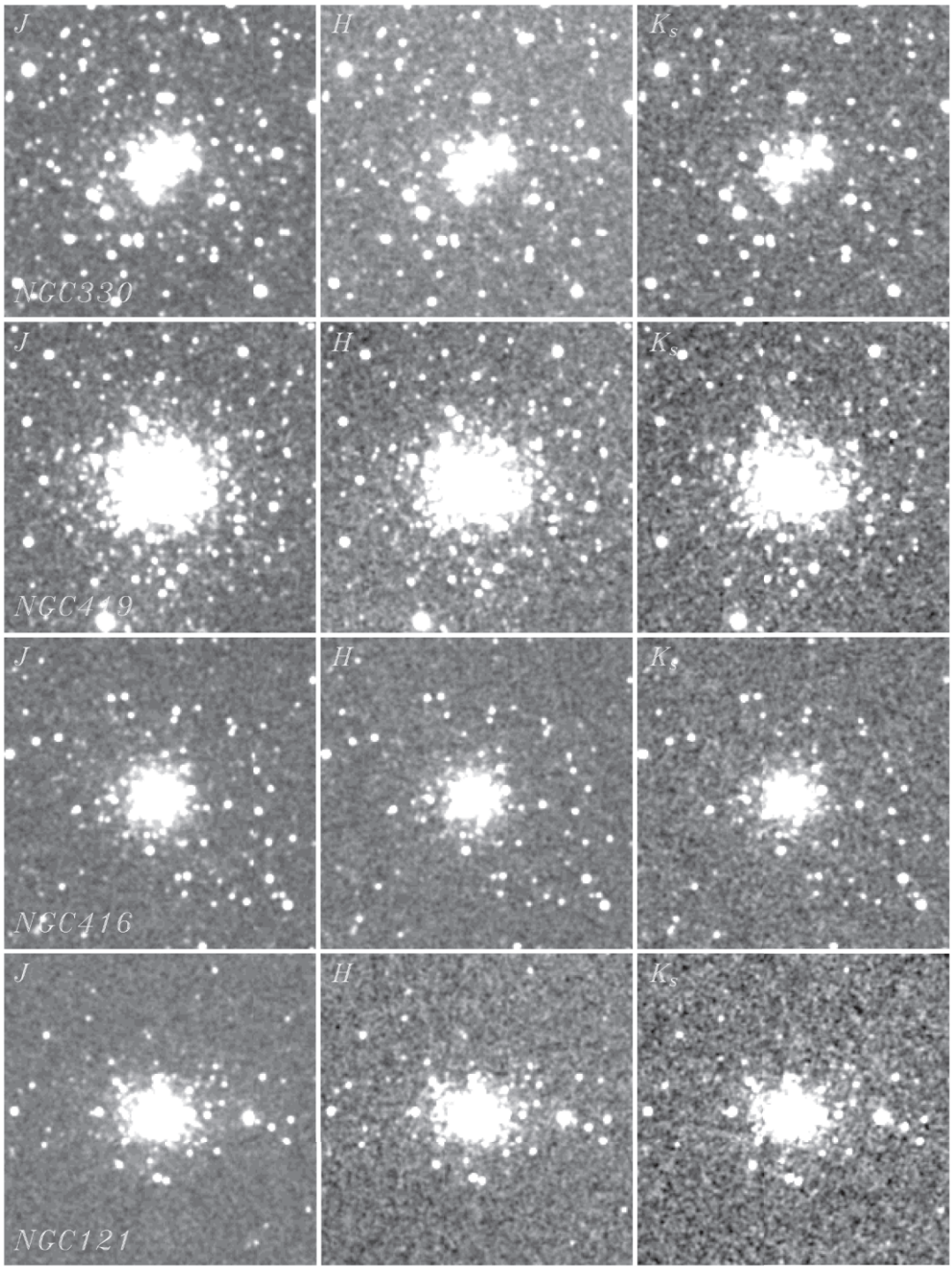

FIG. 1.—*J*, *H*, and K_s images of four SMC clusters. Each image is $200'' \times 200''$, centered on the cluster position derived in the present paper. North is up, and east is to the left. The curves of growth for each of these objects can be found in Fig. 8.

The results were compared with the age of the cluster and the expected absolute visual magnitudes of these stars at the distance to the SMC or LMC. If there was a discrepancy between the measured and expected magnitudes or if such stars were unlikely to be found in a cluster with the given age, they were subtracted. There are several examples of this procedure described in § 2.7.

2.5. *Integrated Cluster Photometry*

The aperture photometry of the clusters was performed with the IRAF APPHOT package on a set of three residual images in each survey band. The images are a result of the application of the DAOPHOT ALLSTAR and the IRAF SUBSTAR procedures on the original atlas frames. In the first of them, all detected point sources were removed (actually, this was the output residual image from ALLSTAR), in the second, the LF of the background field was subtracted from the cluster area using SUBSTAR with an exclude file, containing the stars remaining after the statistical subtraction, and in the third image were contained all the point sources within the photometry aperture. The images were used to measure the flux from the unresolved, background-subtracted,

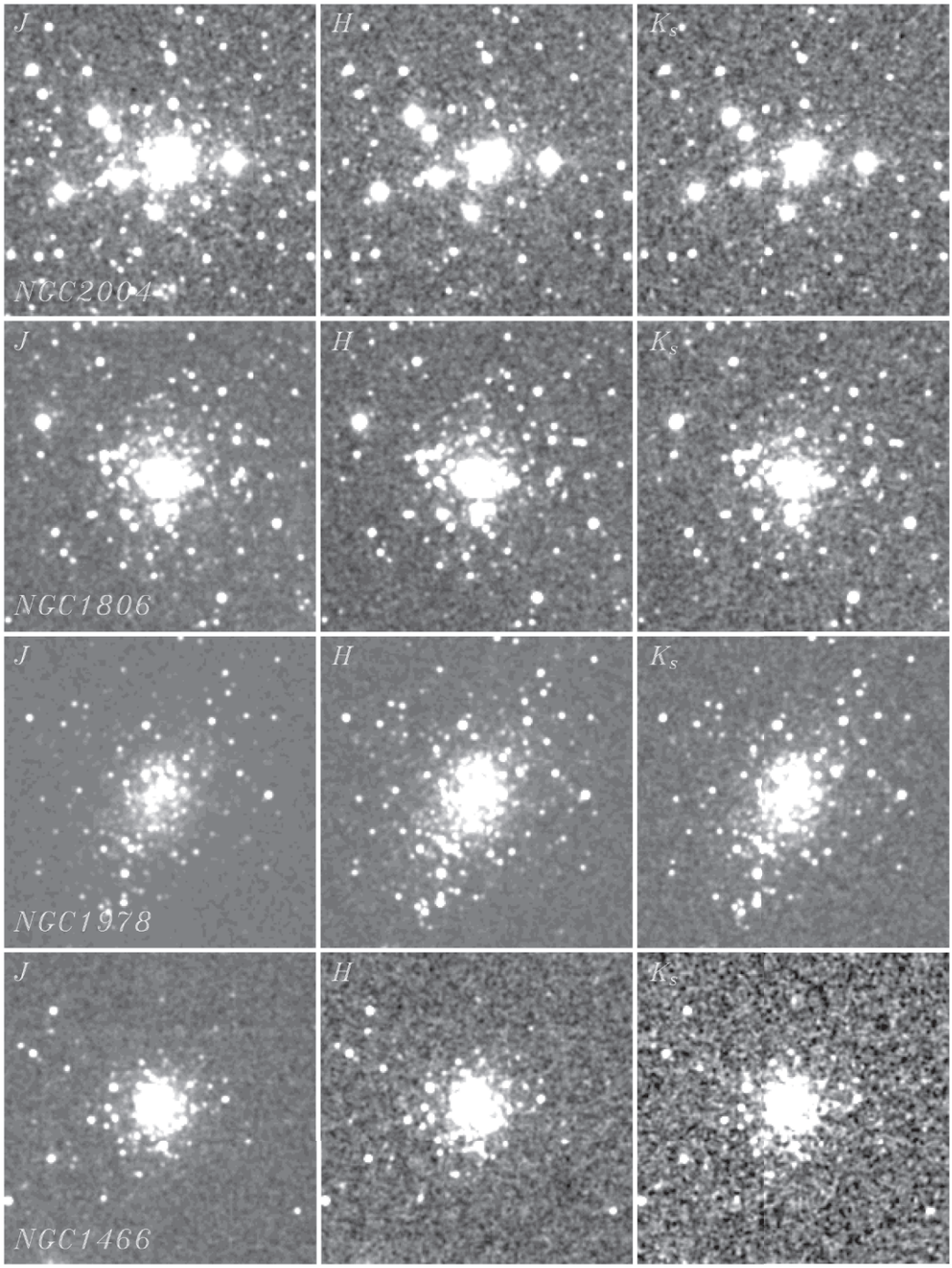

FIG. 2.—*J*, *H*, and K_s images of four LMC clusters. Each image is $200'' \times 200''$, centered on the cluster position derived in the present paper. North is up, and east is to the left. The curves of growth for each of these objects can be found in Fig. 9.

and total flux from the object, using a set of apertures ranging from $1''$ to $100''$ in radius with a step size of $1''$. We computed curves of growth for all sample globular clusters in the three survey bands. The sky background level in each frame was estimated in a sky annulus encircling our largest aperture with a width of at least 10 pixels. The exclusion of the stars outside of the largest aperture prior to the final integrated photometry provided a better estimate of the sky background. In those cases in which the cluster was situated close to the frame edge, we used the largest aperture possible, and the background levels were measured in a nearby region that matched or exceeded the equivalent area of a full background annulus circle.

For each aperture the error introduced by the stochastic fluctuations in the stellar population of the foreground/background was estimated. We computed the LF of objects outside each photometry aperture for each particular object. The corresponding flux was integrated over the entire LF, and the standard deviations of stellar counts were calculated in bins of $\Delta m = 1$ mag. These values were then normalized to the area used for the cluster photometry. Bright stars close to saturation were identified on

TABLE 3
2MASS Atlas Images of MC Clusters

Cluster ID	N	J	H	K_s
		SMC		
NGC 121	3	s4_aJ_asky_981020s0400256.fits	s5_aH_asky_981020s0400256.fits	s6_aK_asky_981020s0400256.fits
NGC 152	3	s7_aJ_asky_980808s0580221.fits	s8_aH_asky_980808s0580221.fits	s9_aK_asky_980808s0580221.fits
NGC 330	2	s4_aJ_asky_980809s0930245.fits	s5_aH_asky_980809s0930245.fits	s6_aK_asky_980809s0930245.fits
NGC 339	3	s7_aJ_asky_980809s0940115.fits	s8_aH_asky_980809s0940115.fits	s9_aK_asky_980809s0940115.fits
NGC 361	2	s4_aJ_asky_981021s0450256.fits	s5_aH_asky_981021s0450256.fits	s6_aK_asky_981021s0450256.fits
NGC 411	3	s7_aJ_asky_981021s0560009.fits	s8_aH_asky_981021s0560009.fits	s9_aK_asky_981021s0560009.fits
NGC 416	1	s1_aJ_asky_980809s1060021.fits	s2_aH_asky_980809s1060021.fits	s3_aK_asky_980809s1060021.fits
NGC 419	3	s1_aJ_asky_980809s1060044.fits	s2_aH_asky_980809s1060044.fits	s3_aK_asky_980809s1060044.fits
NGC 458	2	s4_aJ_asky_981021s0680021.fits	s5_aH_asky_981021s0680021.fits	s6_aK_asky_981021s0680021.fits
Kron 3	2	s4_aJ_asky_980808s0470044.fits	s5_aH_asky_980808s0470044.fits	s6_aK_asky_980808s0470044.fits

Notes.—Table 3 is published in its entirety in the electronic edition of the *Astronomical Journal*. A portion is shown here for guidance regarding its form and content.

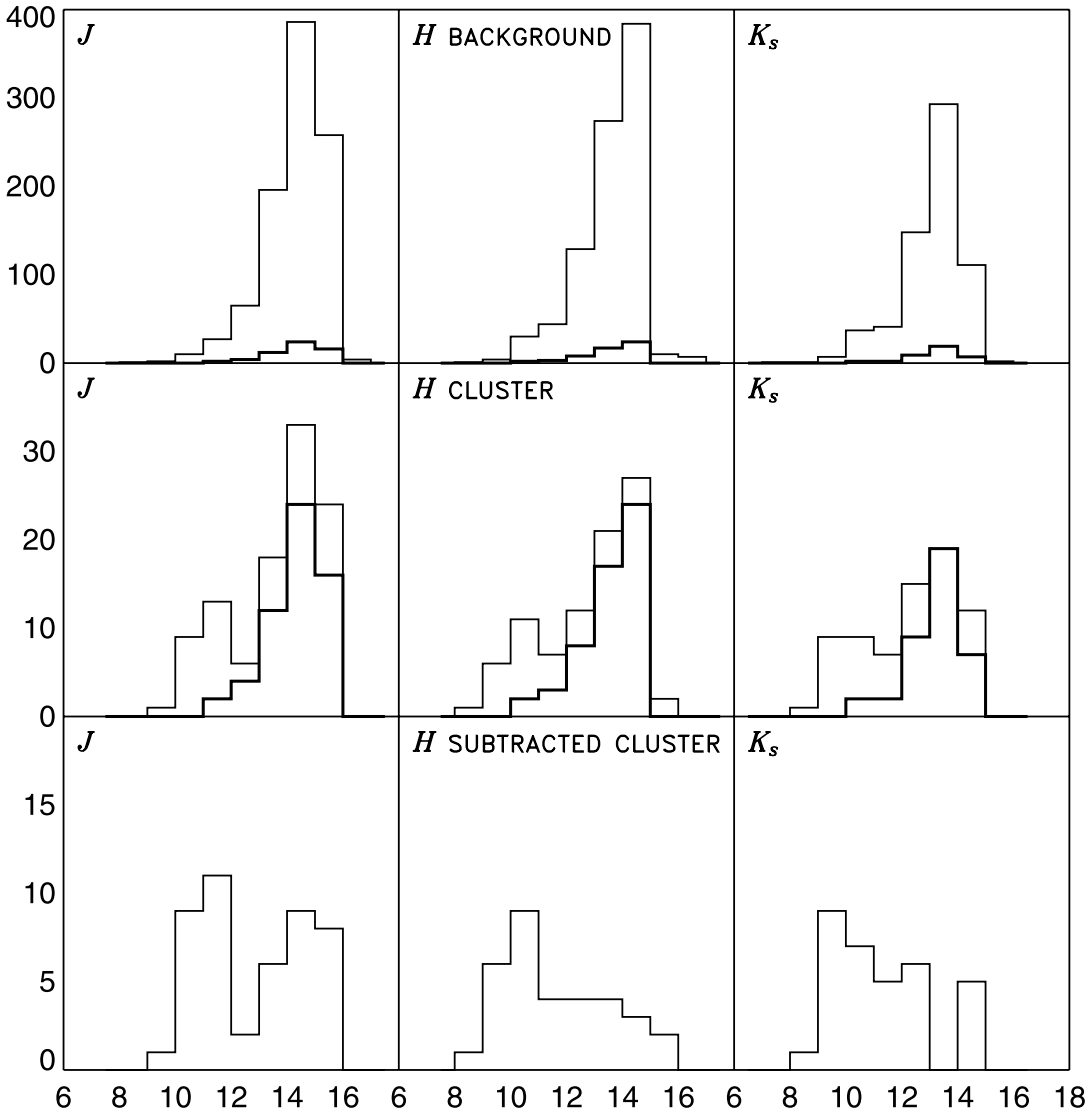

Fig. 3.—LFs for NGC 330 of the background (*top panels*), cluster field (*middle panels*), and cluster field after background subtraction (*bottom panels*). The thick line in the first and second row of panels represents the background LF scaled to the area of the largest aperture.

TABLE 4
PHOTOMETRY OF MC CLUSTERS

Cluster ID (1)	$\alpha_{J2000.0}$ (2)	$\delta_{J2000.0}$ (3)	d (arcsec) (4)	Flag (5)	R (arcsec) (6)	J (7)	J Error (8)	H (9)	H Error (10)	K (11)	K Error (12)
					SMC						
Lindsay 1	00 03 55.2	−73 28 12.4	16.5	BBB	20	14.63	0.06	14.37	0.12	14.97	0.27
	00 03 55.2	−73 28 12.4	16.5	BBB	40	12.60	0.03	12.23	0.04	12.27	0.05
	00 03 55.2	−73 28 12.4	16.5	BBB	60	11.67	0.03	11.29	0.03	11.17	0.04
	00 03 55.2	−73 28 12.4	16.5	BBB	80	10.88	0.02	10.42	0.03	10.30	0.03
	00 03 55.2	−73 28 12.4	16.5	BBB	100	10.52	0.03	10.04	0.03	9.97	0.03
	00 03 55.2	−73 28 12.4	16.5	BBB	120	10.35	0.03	9.87	0.03	9.82	0.03
	00 03 55.2	−73 28 12.4	16.5	BBB	140	10.25	0.04	9.79	0.04	9.73	0.04
	00 03 55.2	−73 28 12.4	16.5	BBB	160	10.09	0.04	9.61	0.04	9.57	0.04
	00 03 55.2	−73 28 12.4	16.5	BBB	180	9.92	0.04	9.40	0.04	9.37	0.05
	00 03 55.2	−73 28 12.4	16.5	BBB	200	9.83	0.05	9.31	0.05	9.30	0.05

NOTES.—Col. (1) is the cluster designation, and cols. (2) and (3) are the right ascension and declination of the position used to center the apertures for the integral photometry. Units of right ascension are hours, minutes, and seconds, and units of declination are degrees, arcminutes, and arcseconds. Col. (4) is the offset of that position with respect to the cluster coordinates in SIMBAD, measured on 2MASS atlas images. Col. (5) contains a flag providing information about the age (first letter), metallicity estimates (second letter), and photometry (third letter) for each cluster. "A" corresponds to a reliable age, metallicity, or photometry, and "B" denotes the cases in which the age and metallicity values are uncertain. When used in the third position, "B" indicates the cases described in § 2.7 or in which the photometry was provided from aperture sizes smaller than 200″. The radii of the apertures used for each measurement are listed in col. (6). The photometry information is given in columns (7)–(12), in the order of the J magnitude and error of photometry in J, and then the same for the other two survey bands H and K_s. The error of the photometry in each band is calculated as the square root of the quadrature sum of the zero-point error, the internal error of the photometry, and the error due to stochastic fluctuations of the background stellar population. Table 4 is published in its entirety in the electronic edition of the *Astronomical Journal*. A portion is shown here for guidance regarding its form and content.

the images and excluded from the photometry prior to the procedures described above. The error values listed in Table 4 in each survey band are the quadrature sum of the photometry errors from APPHOT, the 2MASS zero-point errors, and the calculated background stochastic fluctuations. In general, the errors of our photometry increase as a function of aperture radius and depend on background properties.

Example curves of growth of the photometry for the SMC cluster NGC 411 and LMC cluster NGC 2231 are presented in Figures 4 and 5, respectively. The solid lines show the magnitudes of the clusters after background subtraction. The estimated errors due to stochastic background fluctuations are overplotted with dotted lines. The dashed curves represent the total fluxes from the clusters (without background subtraction), and the unresolved components are plotted with dot-dashed lines. NGC 2231 in Figure 5 also illustrates what could be the effect on the integrated magnitudes of the cluster if there is improper handling of the background subtraction. This cluster lies in a region of relatively high apparent stellar density, and there are several bright stars present. The stochastic fluctuations of the stellar background show the possibility of a severe overestimation of the cluster total magnitude if the influence of the bright stellar objects is not taken into account. Note that the error values in Table 4 are calculated with the bright stars excluded from the background LF. Integrated magnitudes and photometric curves of growth for all star clusters analyzed in this study are available on request from the first author.

2.6. *Extinction Correction*

In order to determine the intrinsic magnitudes and colors of our sample clusters, the measurements must be corrected for the effect of extinction. Cluster extinction values were obtained from three independent studies: Burstein & Heiles (1982), Schlegel et al. (1998), and the Magellanic Clouds Photometric Survey (MCPS; Zaritsky et al. 1997); see Zaritsky et al. (2002) for the SMC and Zaritsky et al. (2004) for the LMC. The study by Burstein & Heiles is based on maps of the H I emission, while the Schlegel et al. maps use *IRAS* DIRBE data on the far-IR sky emission. The corrections provided by Schlegel et al. (1998) are superior to those of Burstein & Heiles (1982) because of the improved spatial resolution and the fact that they estimate the extinction from the dust properties directly, not using H I as an intermediate agent. But there is an important caveat: the Schlegel et al. maps are highly uncertain in the inner regions of the Clouds because their temperature structure was not sufficiently resolved by DIRBE. The most recent development in Magellanic Clouds extinction work is the MCPS data. This survey covers the central $4^\circ \times 4^\circ$ of the SMC and $8^\circ \times 8^\circ$ of the LMC in *UBVI*. The limiting magnitude of the MCPS maps (set primarily by crowding) is $V = 21$ mag. However, these maps cover only the inner body of the Magellanic Clouds, and extinction information for star clusters located in the outer regions is not available.

Extinction estimates based on H I emission and *IRAS* DIRBE dust maps were retrieved for all objects from the NASA/IPAC Extragalactic Database. The values from MCPS were retrieved using the online tools available on the Web site of the project.[5] The MCPS maps provide a statistical approach to the extinction: stellar atmosphere models are fitted to the measured *UBVI* magnitudes of all the stars in a user-defined search radius with good-quality photometry and good model fits (Zaritsky 1999). The distribution of the extinction values is built, and the result of the mean extinction and $\sigma_{\rm ext}$ of the distribution is given. There are different options available, but for the current work we chose to use the estimates based on "cool" stars ($T \leq 10^4$ K) in the search radius. Since cool stars are more homogeneously distributed than hot stars, extinction measurements from cool stars should provide a more representative estimate of the true extinction value. The extinction map of the central region of the LMC, showing all the objects with estimates available from the three studies, is presented in Figure 6. Generally the values from Burstein & Heiles (1982) and Schlegel et al. (1998) are in good agreement but, in most cases, lower than those derived from

[5] See http://ngala.as.arizona.edu/dennis/mcsurvey.html.

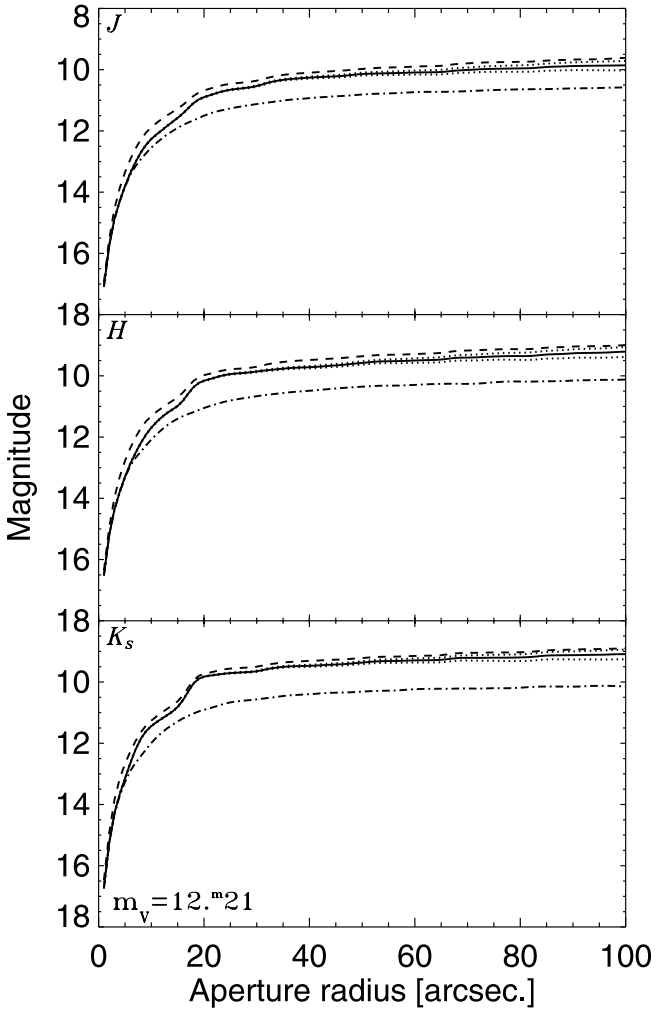

FIG. 4.—Curves of growth in the three 2MASS bands for the SMC cluster NGC 411. The dashed curves represent the total flux from the object (no background/foreground-subtraction applied), and the dot-dashed lines stand for the unresolved components in the atlas images. The solid lines show the background-subtracted curves of growth, and the errors due to the stochastic fluctuations of the background are overplotted with dotted lines. The V photoelectric magnitude with a 62″ diaphragm is taken from Alcaino (1978).

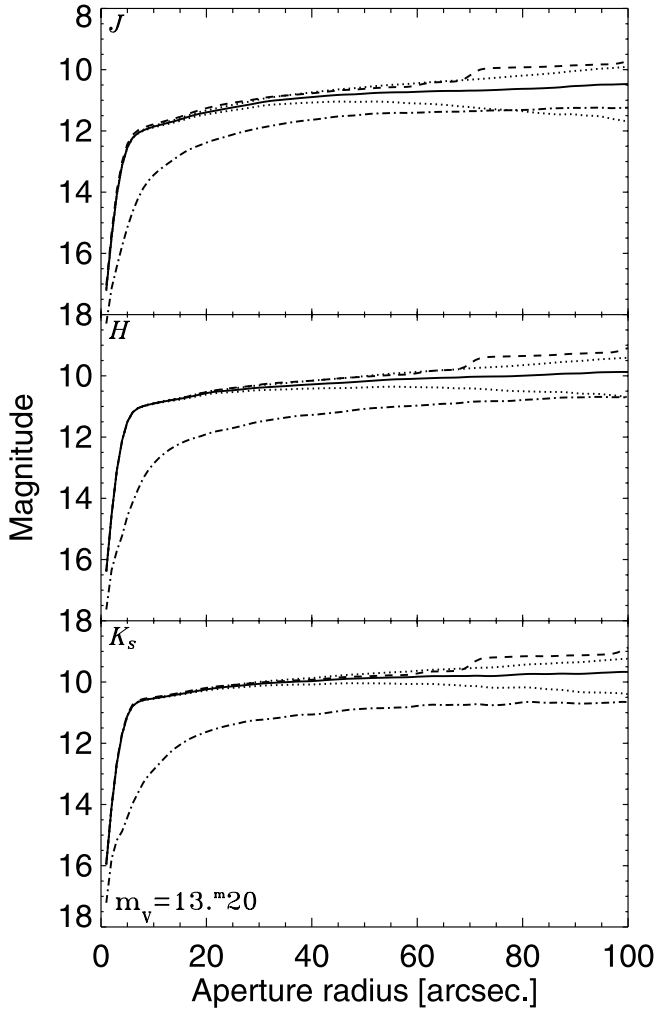

FIG. 5.—Curves of growth in the three 2MASS bands for the LMC cluster NGC 2231. The dashed curves represent the total flux from the object (no background/foreground-subtraction applied); note the clear "bump" due to a foreground star. The solid lines stand for the background-subtracted curves of growth, and the dot-dashed lines for the unresolved components in the atlas images. The errors due to the stochastic fluctuations in the background are overplotted with dotted lines. The values of these errors are quite high because the bright stars in the background field are not excluded from the LF, illustrating the possibility of overestimation of the cluster total magnitude. The photoelectric visual magnitude in a 44″ aperture is taken from van den Bergh (1981).

Zaritsky et al. (2004). Using a search radius of 2′, which is slightly larger than our largest photometry aperture, we achieve a robust estimate of the extinction toward a specific object.

We use the extinction values based on the MCPS maps. In those cases in which no MCPS data are available, we adopt a typical extinction value, derived from all objects with extinction estimates from MCPS. These mean values are derived by fitting the extinction distribution for 40 LMC and 9 SMC clusters with a Gaussian profile (see Fig. 7). The adopted values are $A_B = 0.52 \pm 0.02$ and $A_V = 0.39 \pm 0.02$ for the LMC, and $A_B = 0.22 \pm 0.01$ and $A_V = 0.18 \pm 0.01$ for the SMC. They are higher than the mean values from Schlegel et al., which are $A_B = 0.32 \pm 0.05$ and $A_B = 0.16 \pm 0.03$ for the LMC and SMC, respectively. This result is consistent with the fact that the extinction values for the LMC and SMC listed in Schlegel et al. (1998) only provide lower limits: they only account for Galactic dust, whereas the dust in the Clouds is not taken into consideration. We adopt the extinction law of Bessell & Brett (1988).

To account for the younger stellar population in objects in our sample with log (age) < 8.3, we use the extinction values based on all stars. This approach provides a better estimate than using "hot" stars ($T \leq 10^4$ K) alone, because it reduces the influence of the relatively shallow MCPS U-band photometry.

2.7. *Notes on Individual Objects*

There are a few cases in which the data reduction and photometry differed slightly from the procedure described above. Additional remarks for these clusters are provided below.

NGC 121: There is a relatively bright star located ~60″ west of the center of the cluster. An inspection of 2MASS and optical images (from SIMBAD)[6] showed that it is most likely a foreground star superposed on the cluster. Its magnitudes from ALLSTAR output files are $J = 10.78$, $H = 10.22$, and $K_s = 10.11$. The extinction correction values are taken from Burstein & Heiles (1982) and Schlegel et al. (1998) (we discuss extinction corrections in detail in § 2.6). They are $A_B = 0.15$ and 0.16, respectively, and we use their mean in this analysis. The measured colors are $(J - H)_0 = 0.55$, $(H - K_s)_0 = 0.104$, and $(J - K_s)_0 = 0.65$.

[6] See http://simbad.u-strasbg.fr.

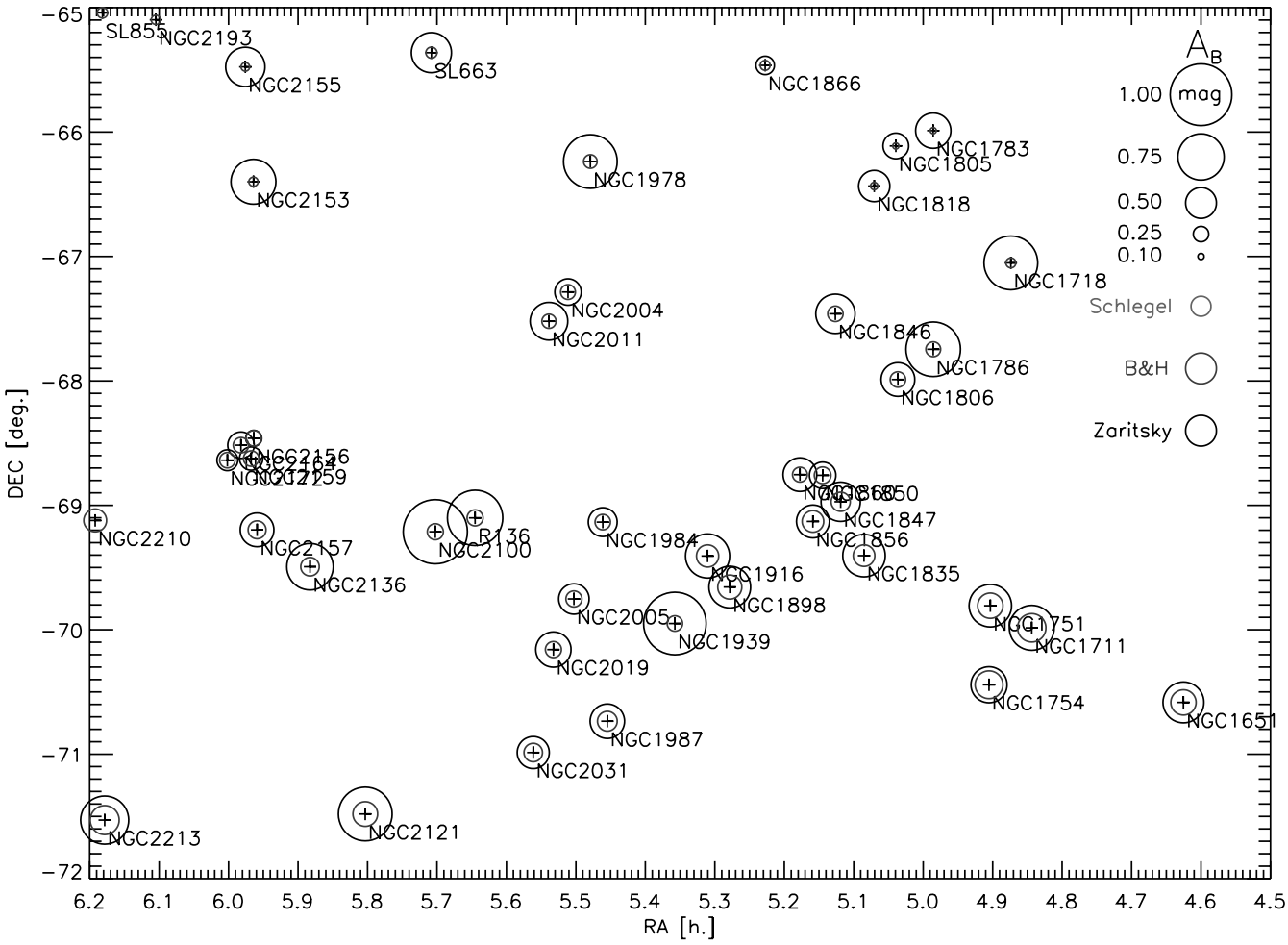

FIG. 6.—Extinction map of the region of the LMC where extinction estimations from the different studies are available for all objects in our sample. The values from Burstein & Heiles (1982) and Zaritsky et al. (2004) are plotted on the map, and the extinction for the LMC given by Schlegel et al. (1998; $A_B = 0.32 \pm 0.05$) is presented with the corresponding symbol size in the legend.

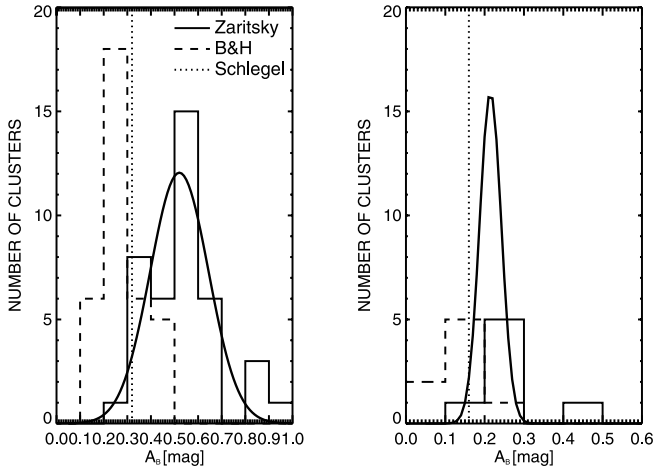

FIG. 7.—Histograms of the extinction values from the studies of Zaritsky et al. (2002) and Burstein & Heiles (1982) for the objects in the central regions of the LMC and SMC. The data are presented in a similar way in both panels. The Gaussian fit of the MCPS data is overplotted on each histogram. The values from Schlegel et al. (1998) for both galaxies are denoted with vertical dotted lines.

Comparing with the results of Ducati et al. (2001) for intrinsic NIR colors of stars shows that its colors are consistent with a K main-sequence, G giant, or supergiant star. In the latter case, a rough derivation of the absolute visual magnitude at the distance of the SMC gives $M_V \approx -7.5$ mag. This is consistent with the star being a supergiant, but it is not likely that such an object can be found in a $\sim$12 Gyr old star cluster. Therefore, we assume that the star belongs to the foreground, and subtract it prior to the final cluster photometry.

NGC 339: This object is relatively close to the edge of the atlas image. The radius of the largest aperture used for photometric measurements is 90″. In all cases in which the maximum size of the aperture was smaller than the typical value of 200″, the last entry for that object in Table 4 is the magnitude measured in the largest aperture used.

NGC 419: There is a bright star in the aperture area $\sim$90″ south-southeast of the center used for photometry. It is clearly visible on the optical frames retrieved from SIMBAD. Given its colors of $J - K_s = 0.410$ and $H - K_s = 0.004$ we conclude that it is most likely a foreground object and subtract it prior to the final measurements.

NGC 458: This young cluster is barely visible in the 2MASS frames, in particular in H and K_s, where the infrared sky background is significantly higher. The curves of growth in these bands start to decline for aperture diameters larger than 80″. We

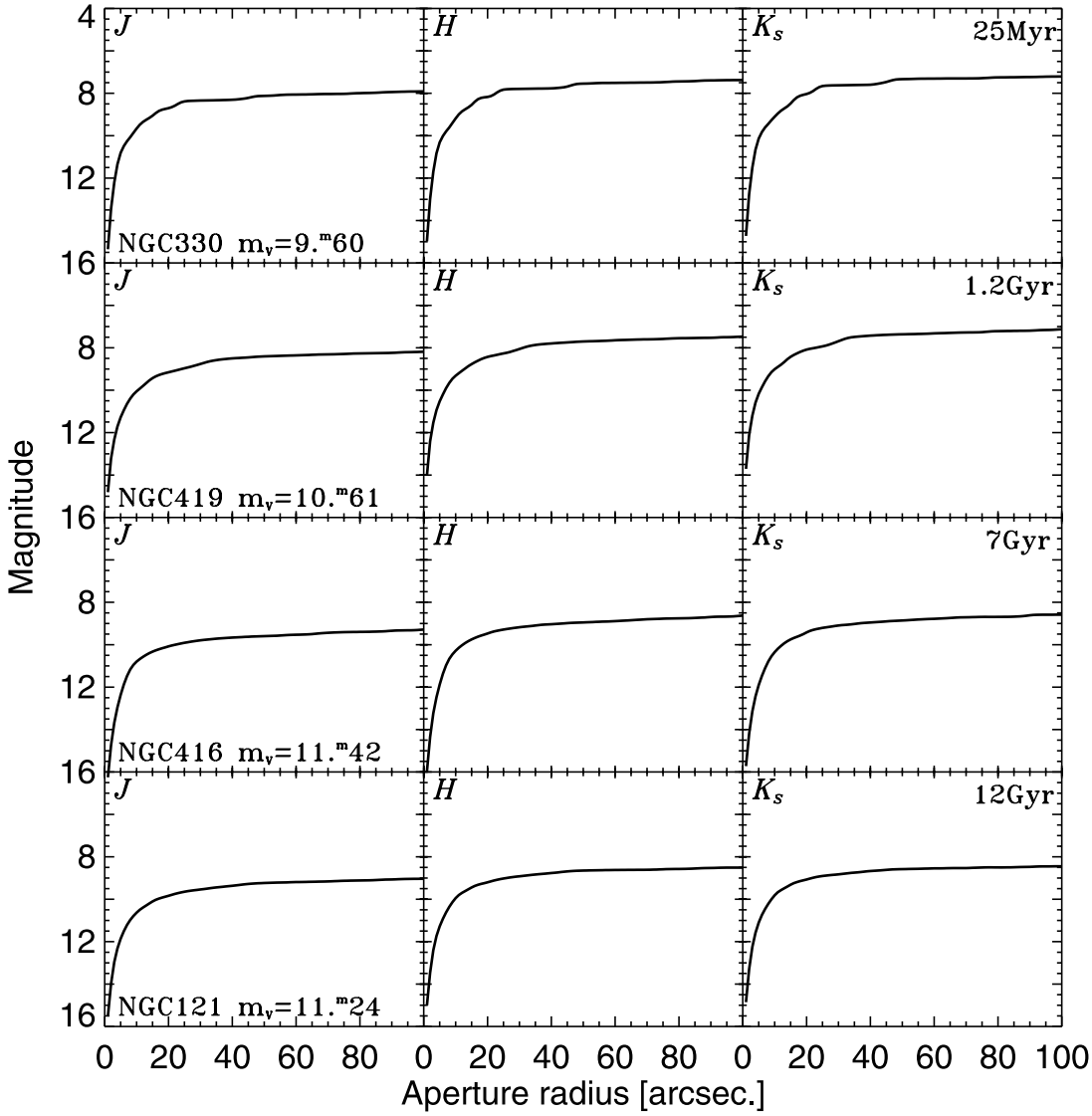

FIG. 8.—Curves of growth for four SMC clusters from our sample. The visual magnitudes are taken from Alcaino (1978). The electrophotometry for all clusters in his study was done with a 62″ aperture. The 2MASS *J*, *H*, and K_s atlas images of these clusters with representable sizes for our largest aperture are shown in Fig. 1.

provide integrated magnitudes only up to 90″ aperture radius, due to the proximity of this cluster to the edge of the atlas image, but the results for the largest radius must be treated with caution.

Lindsay 1: This cluster was split almost equally between two sets of frames. To derive its integrated magnitudes we could not use the usual centering routine, and the center was derived "by eye," accounting for the appearance and position of the cluster in each image. The fluxes from the two halves were measured independently, summed together, and converted into magnitude values. The frames originate from the same scan, acquired on 1998 August 8 between 07:03:03.00 and 07:08:51.00 UT. The regions of the sky in these images were observed at 07:03:43.51 and 07:04:01.38 UT, one after the other. Hence, we averaged the zero points of the frames and used that value for the derivation of the magnitudes. The mean zero points were 20.8522, 20.4090, and 19.8725 in *J*, *H*, and K_s, respectively. The errors of the photometry were estimated in accordance to the described procedure.

NGC 1711: There is a chain of so-called persistence artifacts in close vicinity to the cluster. These features most likely originate from a bright star outside of the current atlas image. Two of them affect the photometry, located at distances of ~47″ and ~66″ from the center. They are well outside of the unresolved cluster component and were measured independently in the residual frames. Their flux was subtracted from the affected apertures before calculation of the magnitude values. The rest of the artifacts were avoided by specifying a larger radius for the background annulus. The resulting errors for this cluster were estimated by taking into account the effect of the artifact removal.

NGC 1754: A bright star is present ~35″ southeast of the center of the cluster, also clearly visible in the visual frames from SIMBAD. The magnitude values derived from our PSF photometry are $J = 9.31$, $H = 8.79$, and $K_s = 8.68$ mag, and the resulting colors are $J - H = 0.52$, $H - K_s = 0.11$, and $J - K_s = 0.63$. This case is similar to NGC 121 in the SMC. The extinction value toward that object was retrieved from the reddening estimator for the LMC on the Web site of MCPS: $A_V = 0.4$. The corrected colors of the star are then $(J - H)_0 = 0.48$, $(H - K_s)_0 = 0.08$, and $(J - K_s)_0 = 0.56$. These colors best match those of a G4 giant from Ducati et al. (2001). The derived absolute visual magnitude is not compatible with the predictions for a G4 giant. The

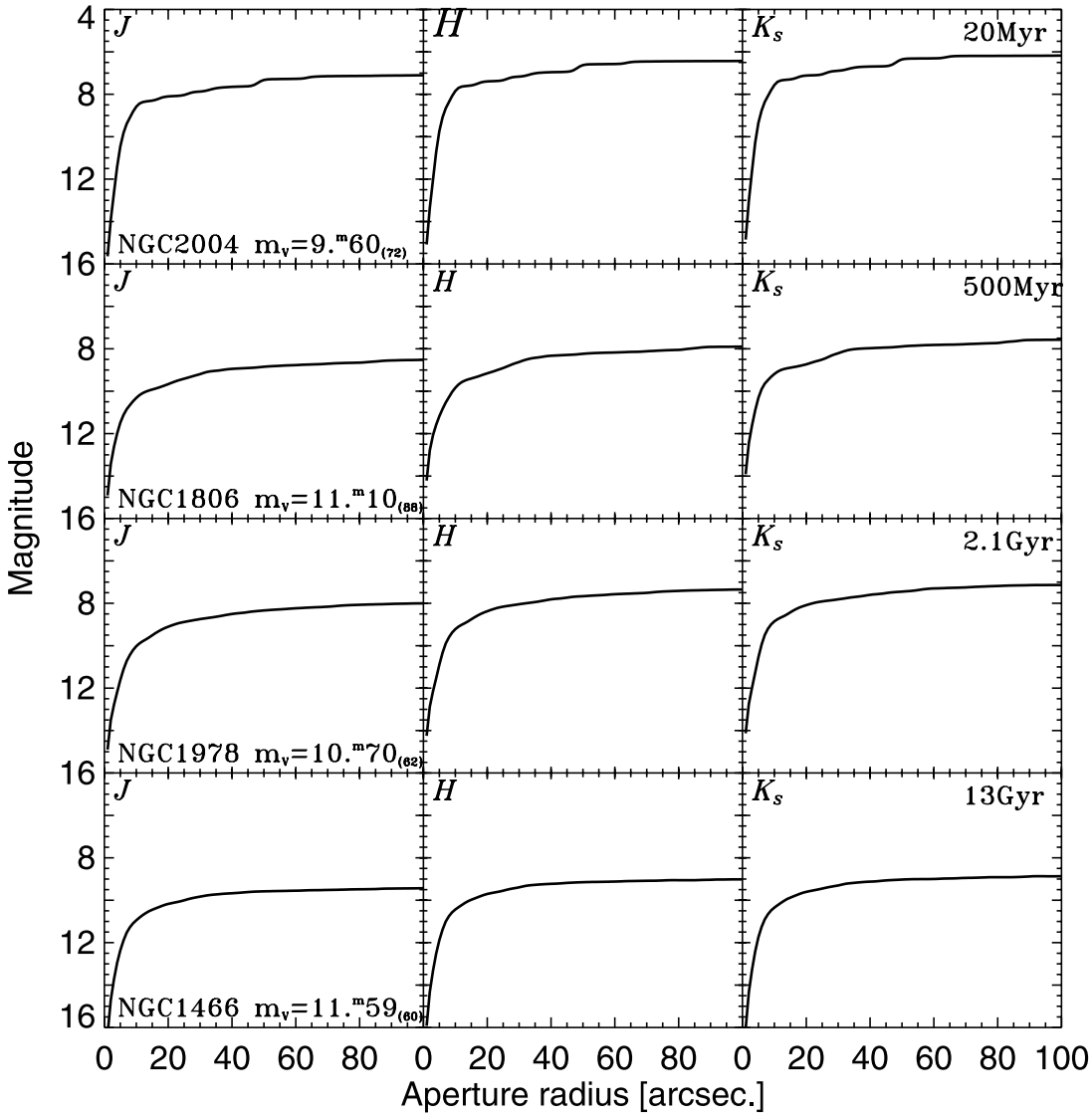

FIG. 9.—Curves of growth for four LMC clusters from our sample. The visual magnitudes are taken from the compilation of Bica et al. (1996). Those data originate from numerous sources and are not homogeneous because of differing detectors and aperture sizes. The apertures used for the measurements of the magnitudes cited on the plots are given in parenthesis. The 2MASS *J*, *H*, and K_s atlas images of these clusters with representable sizes for our largest aperture are shown in Fig. 2.

estimated age of the cluster (~15 Gyr) rules out the possibility that the star is a supergiant. Most likely it is a foreground star, and we exclude it from the measurements of the total cluster luminosity.

NGC 2136: This is one of the most interesting objects in our sample. The cluster is ~100 Myr old, and there is a "satellite cluster" clearly visible in both the visual and NIR images ~ 80″ from the central position derived in the present work. The difference between the coordinates retrieved from SIMBAD and the actual center is 166 pixels in the 2MASS *J* frame. The object is also off-center on the optical frame downloaded from the same database as the coordinates. We conclude that the most probable cause of this discrepancy is a mistake in the coordinates listed in SIMBAD. They are given in Table 2, and the values derived for the centering in the present work are listed in Table 4.

There are two bright stars in the set of apertures used to build the curve of growth. An analysis similar to the case of the stars in the fields of NGC 121 and NGC 1754 led us to the conclusion that the absolute visual magnitudes differ from those expected for luminous stars of these spectral types. We chose at that point to exclude them from the final photometry.

NGC 2153: This object was situated too close to the frame edges on all the sets of atlas images available. We chose those with the best possible location, but the largest aperture radius we could get was still only 40″ before we ran into the frame edge. However, the cluster is compact, and even in that significantly smaller aperture set (compared to that typically used in this work) the curves of growth indicate sampling of the entire flux from the object. In fact, there is some decline observed in *H* for aperture radii larger than 20″. The most likely explanation is local variation in the background, typical for the *H* band. Due to the position of the object the background levels were estimated in a region of the sky close to the cluster. We present the results for the complete set of apertures, but the values of *H* magnitudes must be treated with caution for radii exceeding 20″.

SL 842: This compact cluster is barely detected by 2MASS. Photometry is performed with the entire set of apertures, but the results become highly unreliable for aperture radii exceeding 30″. This aperture appears to encompass the measurable flux from the object, and the results are listed in Table 4.

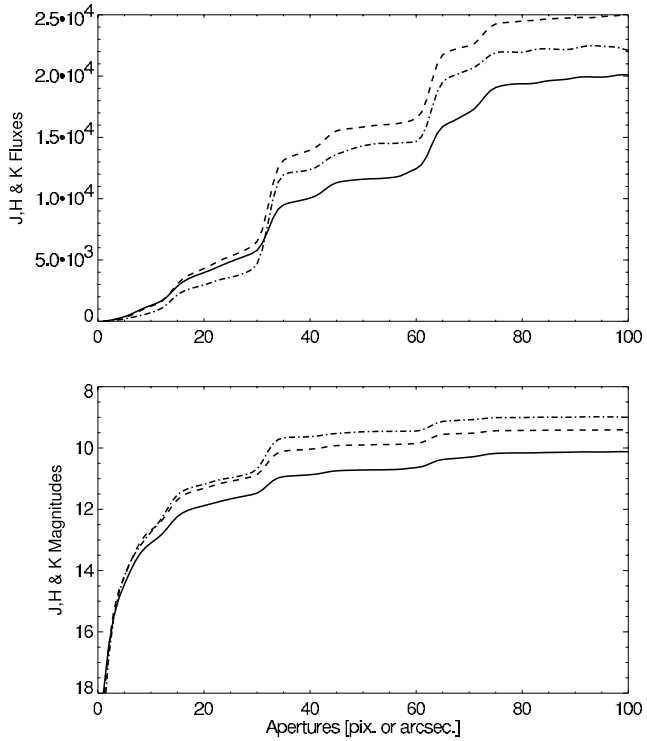

FIG. 10.—Curves of growth in flux units (*top*) and magnitudes (*bottom*) for the LMC cluster NGC 2190 affected by carbon stars. Note the features around $r \sim 30''$ and $60''$ and the steep increase of the flux when the carbon stars enter into the aperture.

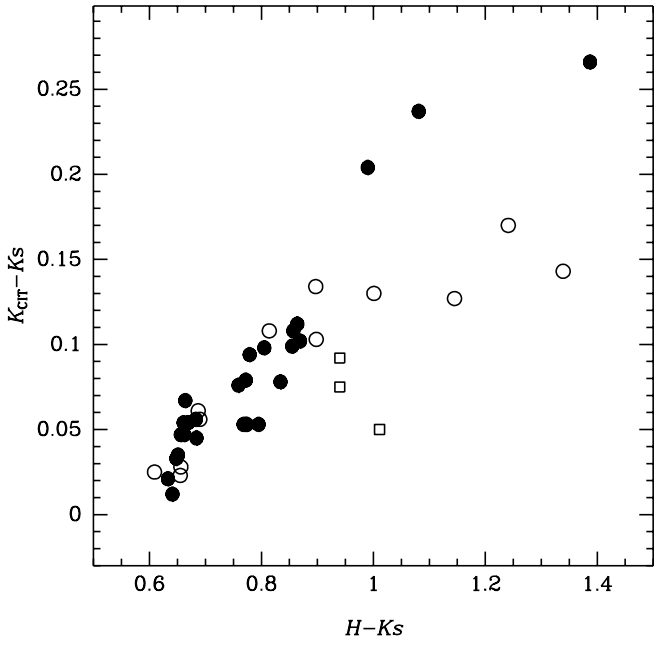

FIG. 11.—Relation between $H - K_s$ and $K_{CIT} - K_s$ for flux-calibrated spectra of late-type stars taken from Lançon & Rocca-Volmerange (1992). Filled circles represent giants of spectral types G5 III–M8 III, open circles represent supergiants of spectral types G2 I–M7 I, and squares represent carbon stars. Note that any difference in calibration from K_{CIT} to K_s between the different spectral types is insignificant for $H - K_s < 0.9$.

SL 855: The cluster is barely visible in the atlas images. The photometry was initially performed with the entire set of apertures. The shape of the curves of growth and inspection of the frames led us to adopt a more conservative approach, and we list only the results to an aperture radius of $10''$.

ESO 121-003: The cluster is faint and extended. It is detected by 2MASS, but the curves of growth are noisy.

3. RESULTS

The results from the integrated 2MASS photometry of the entire Magellanic Clouds cluster sample are presented in Table 4. (The entire table is available in the electronic version of the journal.) A set of typical NIR J, H, and K_s curves of growth of four SMC clusters, ranging in age from ~25 Myr to ~12 Gyr, is given in Figure 8. A closer look at the curve of the youngest cluster, NGC 330, reveals very visible "bumps." These are bright stars contributing to the total light; these are common for young and some of the intermediate-age clusters and are most likely massive young supergiants and carbon stars, which emit significant amounts of light in the NIR. Figure 9 presents curves of growth for LMC clusters also covering a representative age range. The corresponding images of these objects are presented in Figures 1 and 2 for the SMC and LMC, respectively.

The carbon stars present in some intermediate-age clusters are easily distinguished by their colors and luminosity as mentioned by Frogel et al. (1990). They also affect the curve of growth in a typical way, leaving a "fingerprint" of their presence. A good example is the LMC cluster NGC 2190. The curves of growth for this cluster cover the carbon star KDMK 6996 (Kontizas et al. 2001) and another candidate carbon star closer to the cluster center (see Fig. 10). The features at ~$30''$ and $60''$ radii are caused by carbon stars entering the aperture. Note the steeper increase of the curve of growth for K_s compared to those for J and H, and the corresponding features in the flux curves. The carbon star identification is based on the magnitudes and colors from PSF photometry. It is easy to detect the red colors of these objects in the NIR passbands. Their intrinsic colors are expected to be $(J - H)_0 \approx 1$, $(H - K)_0 \approx 1$, and $(J - K)_0 \approx 2$ (Ducati et al. 2001).

3.1. *Comparison with Previous Studies*

We compare our results with the work of Persson et al. (1983) in this section. There are 52 objects in common between our study and their paper: 10 SMC and 42 LMC clusters. The data in that early work were gathered using three different phototubes and an InSb detector system, mounted on three different telescopes: the 1 m Swope and 2.5 m du Pont telescopes of the Las Campanas Observatory and the 0.9 m Cerro Tololo Inter-American Observatory (CTIO) telescope. The observations of Magellanic Cloud clusters were presented in J, H, and K filters of the California Institute of Technology infrared photometric system (CIT) (for details see Frogel et al. 1978).

There are several issues that complicate a direct comparison of the obtained results in the two works: (1) Due to the use of an iris diaphragm at the du Pont and CTIO telescopes at the time, the aperture diameters were only known to $\pm 1''$ (Persson et al. 1983). This could lead to uncertainties in the cluster magnitudes and colors. (2) Another serious problem we became aware of during a series of experiments is related to the centering of the cluster. In many cases the diaphragm apertures used by Persson et al. appear to cover the brightest part of the cluster, because their strategy was to maximize the flux through the aperture. This, however, leaves this technique vulnerable to the effect of stochastic fluctuations of the observed stellar population, in particular for young clusters or clusters that are contaminated by bright stars. Extended clusters without a clear central peak are also

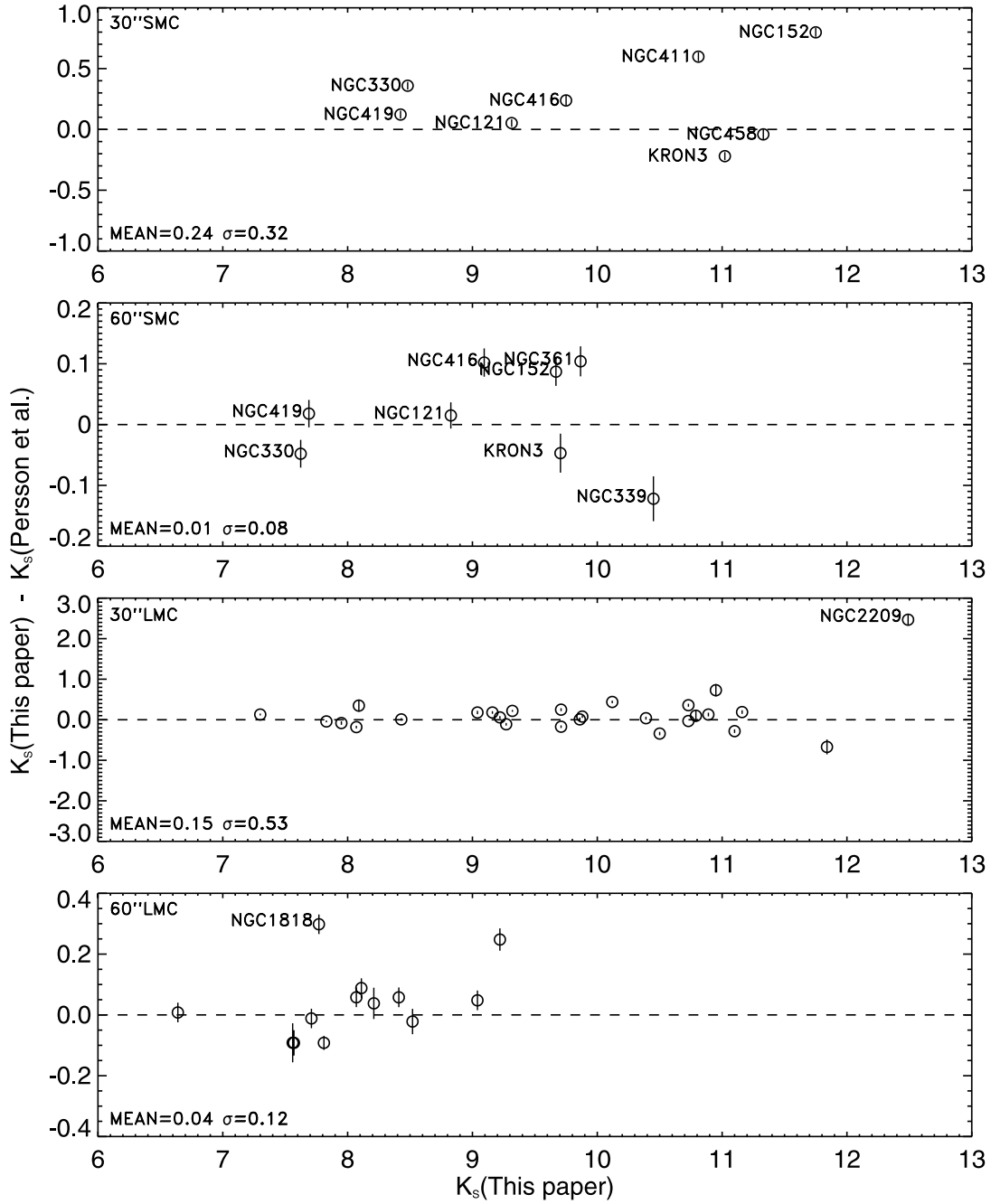

FIG. 12.—Comparison of our 2MASS K_s-band photometry for LMC and SMC clusters with the results of Persson et al. (1983). The dashed lines are the one-to-one relations.

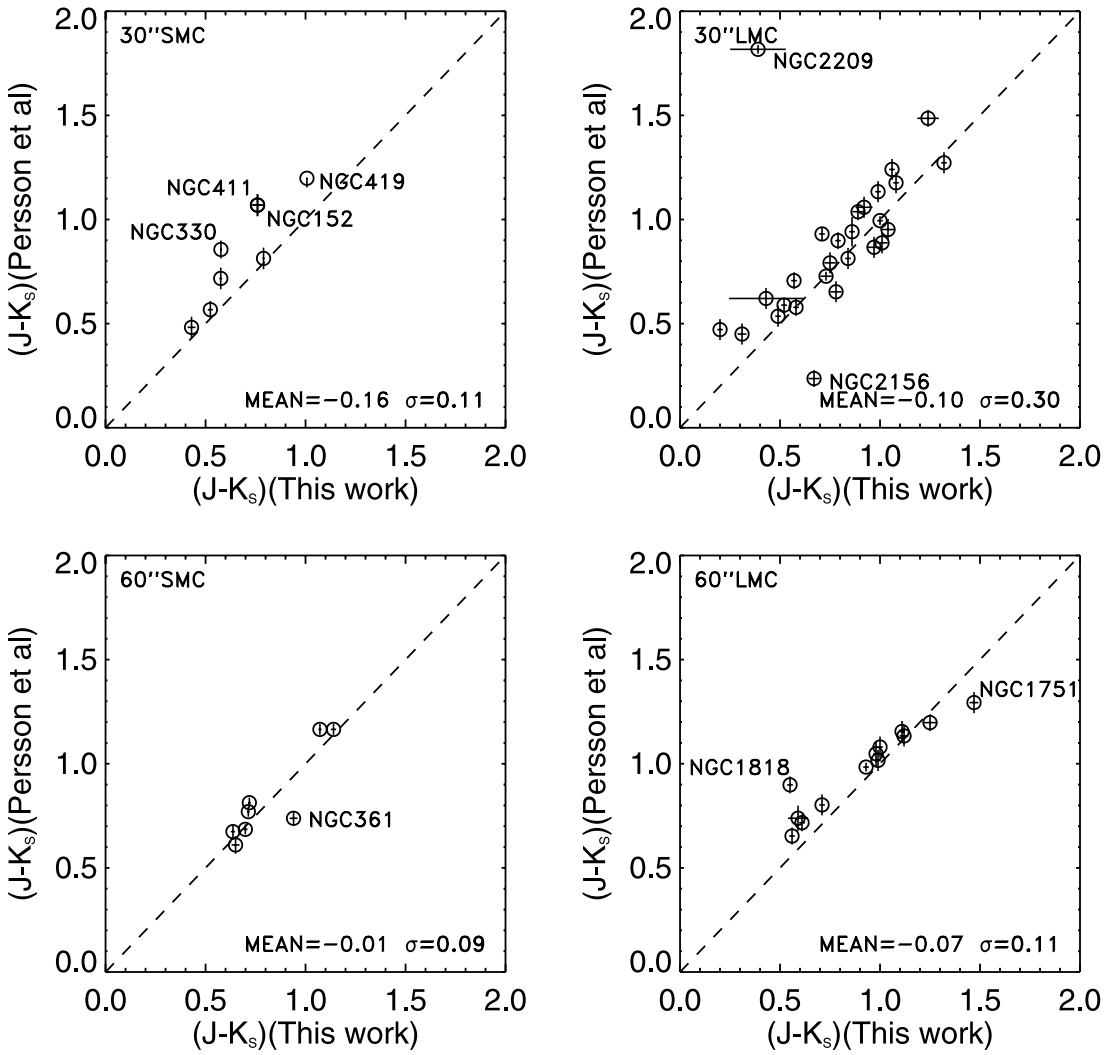

FIG. 13.—Comparison of our 2MASS $J - K$ colors for LMC and SMC clusters with Persson et al. (1983). The dashed lines are the one-to-one relations.

difficult to center using this technique. (3) The cross-calibration between the CIT and 2MASS photometric system was only based on three stars with $(H - K)_{\rm CIT} > 0.5$ (Carpenter 2001). However, one might expect differences in calibration from CIT K to 2MASS K_s for late-type giants as opposed to supergiants or carbon stars [i.e., stars with $(H - K)_{\rm CIT} > 0.5$], since the latter two have stronger CO bandhead absorption features (which affect K much more than they do K_s). As this may be relevant for intermediate-age star clusters whose NIR colors are dominated by light from AGB stars, we tested the significance of this effect by using the SYNPHOT package within IRAF STSDAS along with H- and K-band spectra of late-type giants, supergiants, and carbon stars taken by Lançon & Rocca-Volmerange (1992) and filter throughput curves taken from the work of Skrutskie et al. (2006). As Figure 11 shows, the offset between K and K_s for the different types of late-type stars only starts being significant redward of $H - K_s \sim 0.9$. Since the clusters in our sample all have $H - K_s < 0.9$ (see Table 4), we conclude that color term differences between supergiants and carbon stars do not significantly influence the integrated-light photometry of our clusters, and hence, the cross-calibrations of Carpenter (2001) should be adequate for our purposes.

The CIT K magnitude values, as well as the $(J - K)$ and $(H - K)$ colors from Persson et al. (1983), were thus converted into the 2MASS system by using the transformation equations derived by Carpenter (2001).[7] The comparison plots between K_s magnitudes and the colors for the SMC clusters in common between our work and Persson et al. are presented in Figures 12–14. The mean offsets between the K_s magnitude values from the two studies are 0.13 ($\sigma = 0.26$) and 0.11 ($\sigma = 0.44$) for the SMC and LMC, respectively. For the $(J - K_s)$ color we calculated mean offsets of -0.08 ($\sigma = 0.13$) and -0.08 ($\sigma = 0.25$) for the SMC and LMC, respectively. The $(H - K_s)$ mean offsets for the two galaxies are -0.06 ($\sigma = 0.08$) and -0.09 ($\sigma = 0.16$).

The largest differences appear in the case of NGC 152 situated in the SMC and NGC 2209 in the LMC. If we can explain the nature of these discrepancies it is plausible to assume that it is possible to explain the smaller offsets arising for the rest of the objects in the sample as well.

To investigate this in more detail we plot the J, H, and K_s frames of NGC 152 in Figure 15 (*left panels*). The images are centered on the cluster position derived in this paper (as explained above). To simulate the measurements of Persson et al. (1983), who maximized the count rate received through their single-channel detector, we used an aperture of their size and let

[7] The most recent update of the transformations is available online at http://www.astro.caltech.edu/~jmc/2mass/v3/transformations/.

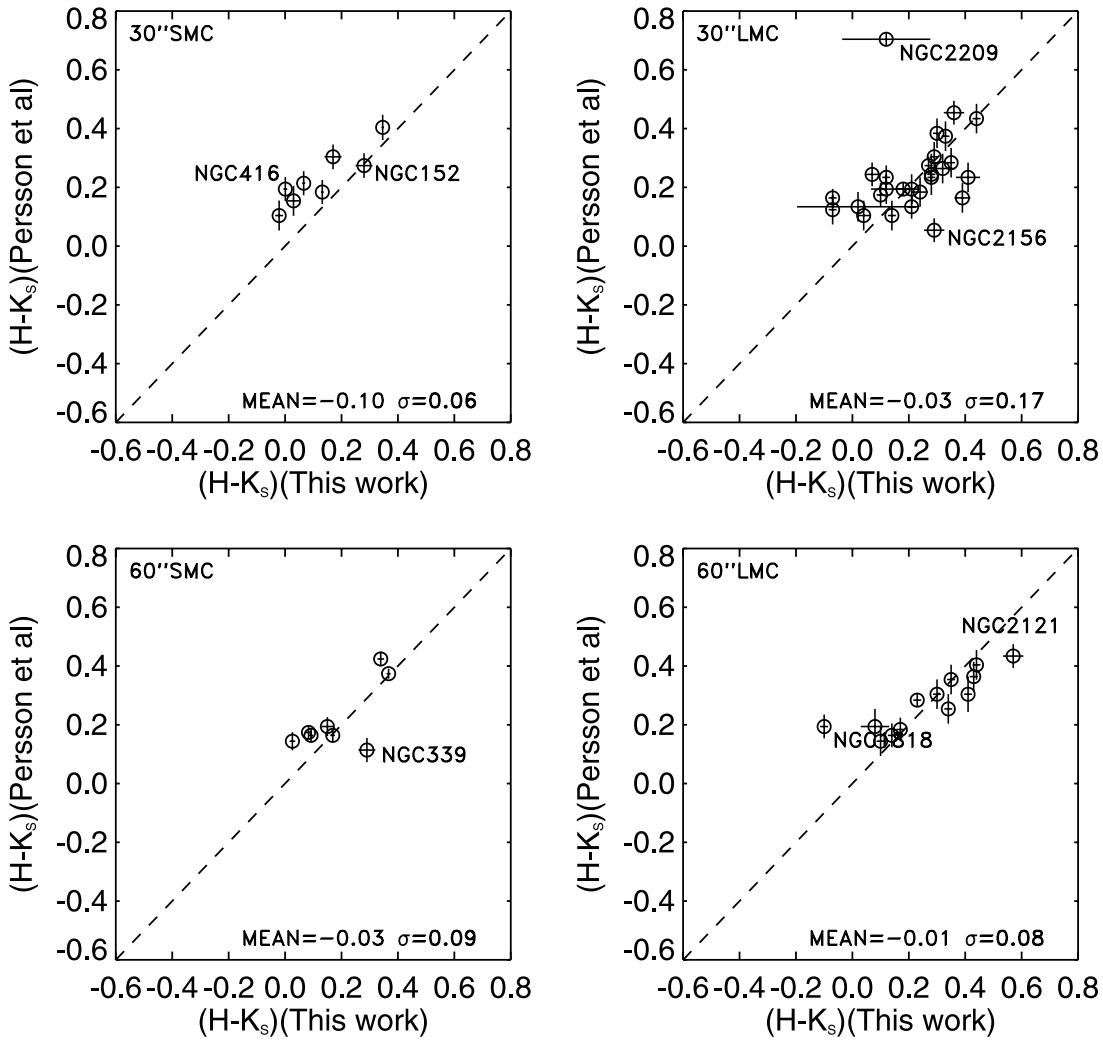

FIG. 14.—Comparison of our 2MASS $H - K$ colors for LMC and SMC clusters with Persson et al. (1983). The dashed lines are the one-to-one relations.

its center drift across a $40'' \times 40''$ subimage located around the center position of our apertures. The step size was 1 pixel (or $1''$), and after the row or column was completed, the aperture center moved to the next one until the entire section was scanned. The measurement with the maximal flux value is assumed to be the center of that aperture in Persson et al. (1983). These simulations were done for each passband independently. The results are listed in Tables 5 and 6. For illustration purposes, we plot the apertures used in our study and the reproduction of those used by Persson et al. together in Figure 15. NGC 152 is an intermediate-age SMC cluster, and there are several bright red stars that dominate the flux in the NIR. (Their presence was also noted by Persson et al.) The faintness of the cluster, the bright stars, and the extended nature of the cluster render the centering extremely difficult for single-channel photometry. The problem is most serious for the smaller aperture, but there is a better agreement for the bigger one. The results of the comparison are shown in Table 5.

NGC 2209 is the most extreme example of differences between our study and that of Persson et al. (1983), amounting to 2.5 mag in the K band. The 2MASS images of this cluster are shown in the right panels of Figure 15. The object is a faint cluster with an age of $\sim$1 Gyr. There are two bright stars dominating the flux, which are carbon stars identified as W46 and W50 by Walker (1971). Persson et al. note that they may affect the centering of their aperture, and therefore likely the results of their photometry, which was performed with a single $30''$ aperture. The offsets of Persson's aperture centers, reproduced by maximal flux experiments, are between 10.5 and 17.5 pixels away from our position, depending on the passband used.

The magnitude and color values listed in Table 2 of Persson et al. (1983) and the curves of growth from our work (presented in Fig. 16) suggest that the flux of the carbon stars in NGC 2209 affects the total cluster magnitudes of Persson et al. To test our simulated position of Persson et al.'s aperture, we converted the magnitudes of Persson et al. (1983) to the 2MASS system and compared them with the corresponding values from our work after recentering our aperture on the simulated position used by Persson et al. The results are presented in Table 6. There is good agreement between K_s magnitudes and $H - K_s$ colors; $J - K_s$ is a little off, but there still is good agreement at the 3 σ level. The most probable reason is a slight difference in the J magnitude values. This is not surprising taking into account that the J-band magnitudes could be affected by rapid variations of the water vapor content in the atmosphere. In this particular case the differences between our results and the photometry of Persson et al. are mainly caused by centering problems. We are taking into account only the photometric uncertainty and the errors of the 2MASS zero points in the analysis above. Due to

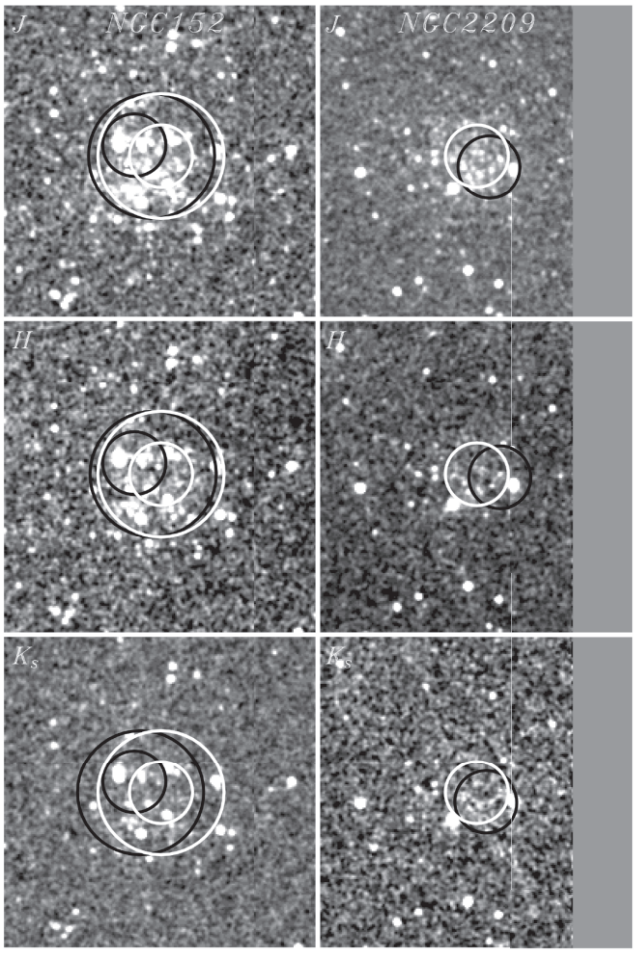

FIG. 15.—2MASS images of NGC 152 and NGC 2209. North is up, and east is to the left. The images are centered on the positions of our apertures, and the size of each one is 200″ square. The gray regions in the right panels indicate that the object is close to the edge of the atlas image. The reproduced apertures of Persson et al. (1983) are plotted in black, and the corresponding apertures from our work are shown in white.

the presence of several relatively bright stars in the background field and the low signal from the cluster, the errors associated with the stochastic fluctuations in the stellar background are quite high. If we take them into account, there is much better agreement between the magnitudes and colors reproduced by our experiment and the values of Persson et al. (1983).

In general, we were able to achieve agreement between our results and those of Persson et al. by assuming a center location for their measurements that is significantly off the "true" center of the cluster in question. The centering discrepancies are smaller for the larger apertures but still large enough to alter the total magnitudes significantly.

Figure 12 is perhaps the best illustration of the effects mentioned above. The total magnitudes of the clusters in Persson et al. (1983) for the 30″ aperture compared to the data in the present paper are underestimated for six of eight objects, and the most probable explanation is centering of the aperture over the brightest part of the cluster population. There is an overestimate in the case of Kron 3, which is a little surprising taking into account the compact nature and the shape of the object. On the other hand, a more careful inspection shows that if the aperture is placed on the geometric center of Kron 3, it is not sampling the most luminous part of the stellar population. In general we have good agreement for the compact and bright clusters, residing in regions of relatively homogeneous foreground or Magellanic Clouds stellar population (e.g., NGC 419 and NGC 121), especially for the larger 60″ aperture. This is also the case for NGC 458, a faint cluster measured by Persson et al. only in a single 30″ aperture. The values of the $J - K_s$ and $H - K_s$ colors of the clusters for the smaller 30″ aperture are systematically higher in Persson et al. The observed trend is also consistent with the expected results from the flux maximization.

Kyeong et al. (2003) presented two-dimensional NIR imaging of a smaller sample of 28 LMC clusters. Their observations were conducted in 1996 December with the CASPIR instrument at the 2.3 m telescope of the Siding Spring Observatory. The clusters were observed in the *JHK* passbands of the South African Astronomical Observatory NIR system. The flux from the background fields was subtracted from the flux measured in the photometry aperture. The authors took advantage of their imaging data to determine the centers of the objects by visual inspection and used them to measure the integrated magnitudes of the clusters in 11 concentric apertures. Unfortunately, the center positions were never published, so it is impossible to provide a detailed comparison between our photometry and the values in the earlier work. We transformed the values of the *J*, *H*, and *K* total magnitudes for their largest aperture ($D = 100''$) into 2MASS magnitudes for the 22 objects in common, using the work of Carpenter (2001). The comparison between the data sets showed mean offsets (by means of difference between our magnitudes and the values of Kyeong et al.) of -0.10 ± 0.05, -0.06 ± 0.04, and 0.00 ± 0.03 in *J*, *H*, and K_s, respectively. An inspection of the observing

TABLE 5
COMPARISON PHOTOMETRY OF NGC 152

Filter ID or Color (1)	*D* (2)	*X* (3)	*Y* (4)	Offset (5)	Reproduced Values (6)	Persson et al. (1983) (7)
K_s	30	348	159	18.5	10.53 ± 0.02	10.95 ± 0.03
$J - K_s$	30	348	159	18.5	1.14 ± 0.03	1.07 ± 0.05
$H - K_s$	30	348	159	18.5	0.39 ± 0.03	0.27 ± 0.05
K_s	60	353	152	13.0	9.54 ± 0.01	9.58 ± 0.02
$J - K_s$	60	353	152	13.0	1.07 ± 0.02	1.17 ± 0.02
$H - K_s$	60	353	152	13.0	0.38 ± 0.01	0.37 ± 0.03

NOTES.—Col. (1) is the filter ID or color being compared with the results from Persson et al. (1983). Col. (2) shows the aperture used for that comparison, in arcseconds. Cols. (3) and (4) show the atlas image coordinates of the recovered aperture centers based on the maximum throughput experiments. The offsets in pixels (or arcseconds) of these positions from the aperture center used in the present work are listed in col. (5). Col. (6) shows the magnitude or color values measured on the 2MASS images using recovered aperture positions from Persson et al. (1983). The corresponding values from Persson et al. transformed into the 2MASS magnitude system by the transformation equations of Carpenter (2001) are listed in col. (7).

TABLE 6
COMPARISON PHOTOMETRY OF NGC 2209

Filter ID or Color (1)	D (2)	X (3)	Y (4)	Offset (5)	Reproduced Values (6)	Persson et al. (1983) (7)
K_s	30	461	457	17.5	10.04 ± 0.02	10.02 ± 0.03
$J - K_s$	30	461	457	17.5	1.68 ± 0.03	1.81 ± 0.02
$H - K_s$	30	461	457	17.5	0.67 ± 0.03	0.70 ± 0.03

NOTES.—Col. (1) is the filter ID or color being compared with the results from Persson et al. (1983). Col. (2) shows the aperture used for that comparison, in arcseconds. Cols. (3) and (4) show the atlas image coordinates of the recovered aperture centers based on the maximum throughput experiments. The offsets in pixels (or arcseconds) of these positions from the aperture center used in the present work are listed in col. (5). Col. (6) shows the magnitude or color values measured on the 2MASS images using recovered aperture positions from Persson et al. (1983). The corresponding values from Persson et al. transformed into the 2MASS magnitude system by the transformation equations of Carpenter (2001) are listed in col. (7).

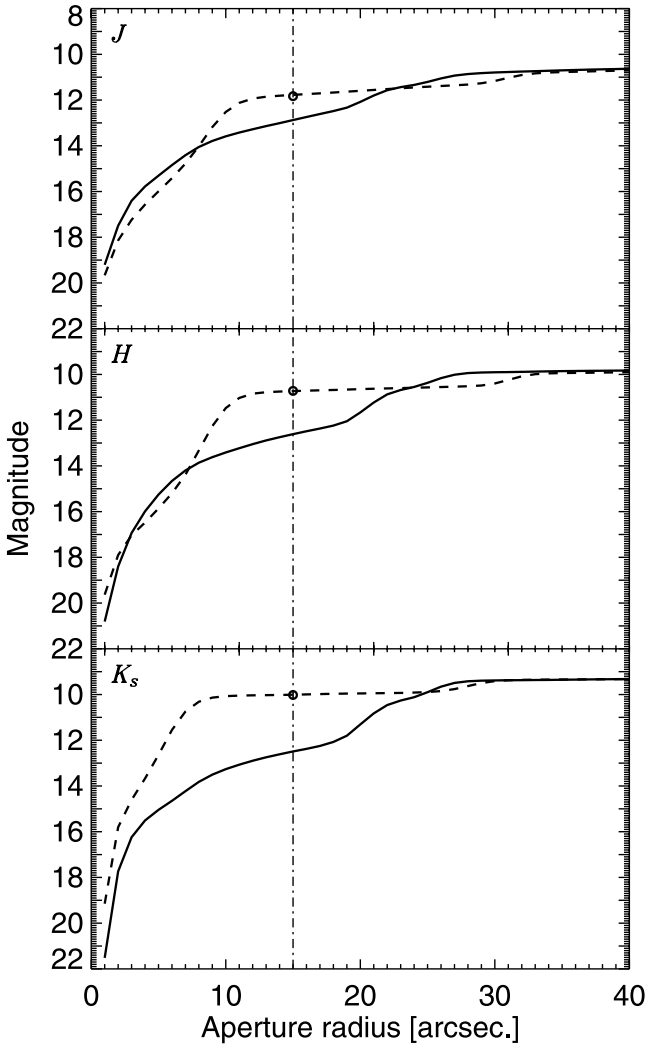

FIG. 16.—J, H, and K_s curves of growth for NGC 2209. The solid lines illustrate our photometry, and the dashed lines stand for the photometry performed with the reproduced centering of Persson et al. (1983). The dot-dashed lines show the 30″ aperture diameter. The points represent magnitude values from Persson et al., and their error bars are compatible with the point size. Note the good agreement between the measurements for larger apertures, showing that the large discrepancies in $D = 30''$ are due mostly to the different centering.

log published in their Table 2 revealed notes about nonphotometric conditions concerning clusters observed during two of the nights. This is a possible explanation for the larger differences between our photometry and the results of Kyeong et al. in the J and H bands, which are much more affected by rapid changes of the atmospheric transition and water vapor content.

3.2. *Comparison with the 2MASS Extended Source Catalog*

The XSC processor in the 2MASS pipeline was designed to provide a flux measurement of the diffuse light of extended sources such as distant galaxies. As described in Jarrett et al. (2000), the XSC processor masks out point sources and substitutes the flux in the masked pixels with the surface brightness of the underlying diffuse light. When applied to star clusters in the Magellanic Clouds, one can therefore expect the XSC processor to eliminate stars that are actually genuine members of the star clusters, some of which contribute significantly to the total flux. As shown in Figure 17, we indeed find that the XSC magnitudes (which are given for 11 concentric circular apertures) are in very good agreement with our photometry of the *unresolved* component of the clusters. However, as the *total* magnitudes of the clusters are significantly brighter than this, we discourage use of the XSC for partially resolved targets such as those considered here.

4. SUMMARY AND CONCLUSIONS

We present a highly uniform data set of integrated J, H, and K_s magnitudes for 75 star clusters in the Magellanic Clouds, using 2MASS survey data. There are reliable age and metallicity estimates available in the literature for the vast majority of the objects in the sample. This is the first extensive NIR survey of the clusters in these galaxies since the single-channel photometry of Persson et al. (1983). Comparing the results of their photometry with the magnitudes from our infrared array curve-of-growth measurements, we find significant differences for some objects, which we can reproduce as being due to centering problems in the early Persson et al. study.

Keeping in mind that the Persson et al. (1983) results were used to calibrate some of the most recent SSP models (Bruzual & Charlot 2003; Maraston 2005), we suggest that the photometry derived in the present work be used to calibrate and improve the existing and future SSP models in the NIR part of the spectrum. We intend to perform a detailed comparison with the predictions of a set of SSP models in a forthcoming paper, using new *VRI* optical data from Goudfrooij et al. (2006).

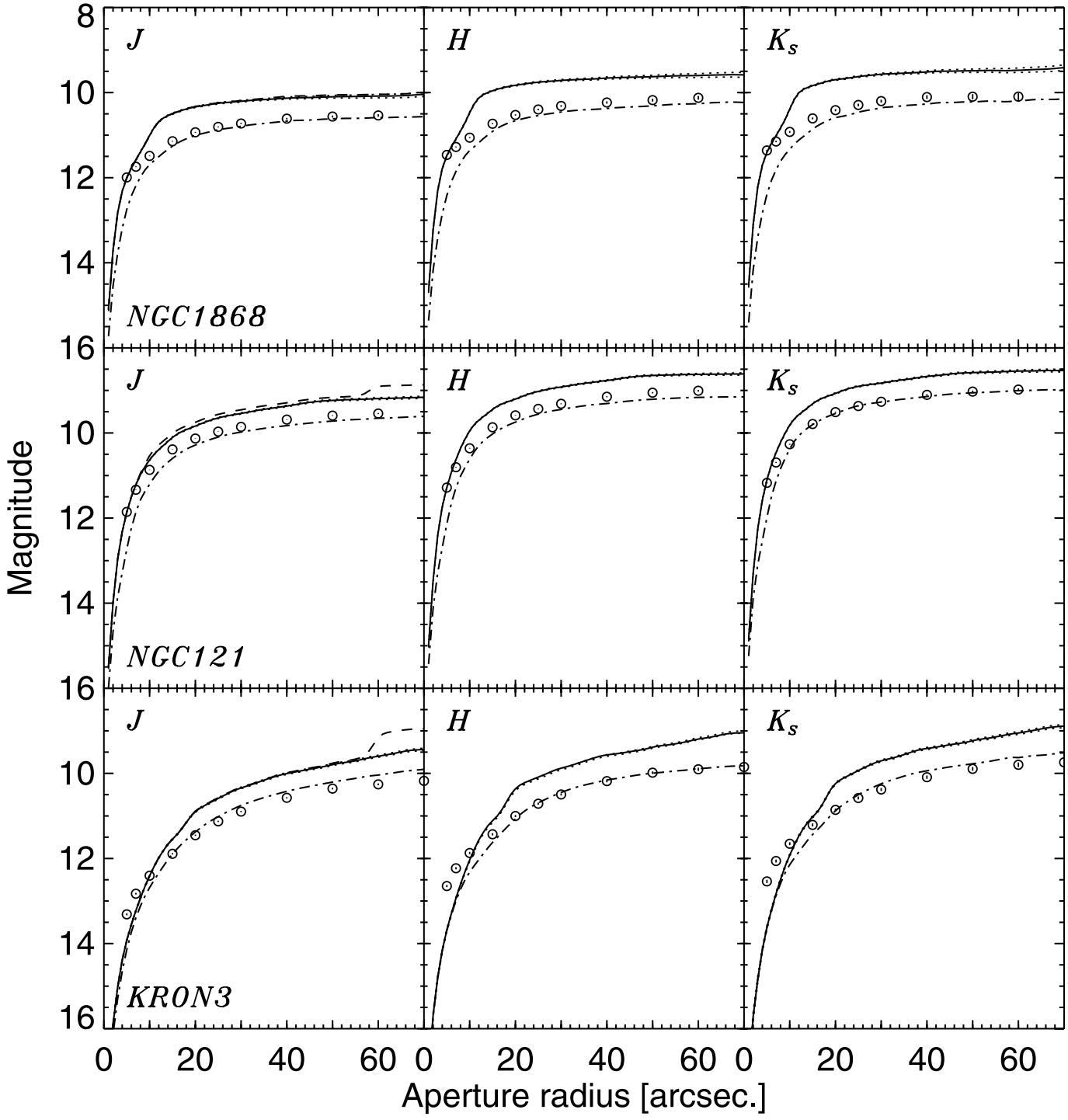

FIG. 17.—Comparison between our photometry (*solid lines*) and 2MASS XSC values (*circles*). The errors are comparable to the thickness of the lines. The total signal from the clusters is shown for clarity only in *J*. XSC values are in much better agreement with the unresolved component (*dot-dashed lines*). The differences in the case of Kron 3 could be attributed to the centering of XSC apertures on the peak *J* pixel.

The authors would like to thank the anonymous referee for helpful suggestions and comments that improved the paper. The authors are thankful to Dennis Zaritsky and his collaborators for the kind and quick response to the inquiry about the MCPS extinction estimation tool and for providing access to their online utility. This publication makes use of data products from the Two Micron All Sky Survey, which is a joint project of the University of Massachusetts and the Infrared Processing and Analysis Center/California Institute of Technology, funded by the National Aeronautics and Space Administration and the National Science Foundation. This research has made use of the NASA/IPAC Extragalactic Database, which is operated by the Jet Propulsion Laboratory, California Institute of Technology, under contract with the National Aeronautics and Space Administration. Support for this work was provided in part by NASA through a *Spitzer Space Telescope* program, through a contract issued by the Jet Propulsion Laboratory, California Institute of Technology, under a contract with NASA. Support for this work was also provided in part by the Space Telescope Science Institute Director's Discretionary Research Fund.

REFERENCES

Alcaino, G. 1978, A&AS, 34, 431
Alves, D. R. 2004, NewA Rev., 48, 659
Alves, D. R., & Sarajedini, A. 1999, ApJ, 511, 225
Beasley, M. A., Hoyle, F., & Sharples, R. M. 2002, MNRAS, 336, 168
Bessell, M. S., & Brett, J. M. 1988, PASP, 100, 1134
Bica, E., Claria, J. J., Dottori, H., Santos, J. F. C., & Piatti, A. E. 1996, ApJS, 102, 57
Bica, E., Geisler, D., Dottori, H., Clariá, J. J., Piatti, A. E., & Santos, J. F. C. 1998, AJ, 116, 723
Bruzual, G., Barbuy, B., Ortolani, S., Bica, E., Cuisinier, F., Lejeune, T., & Schiavon, R. P. 1997, AJ, 114, 1531
Bruzual, G., & Charlot, S. 2003, MNRAS, 344, 1000
Bruzual A., G., & Charlot, S. 1993, ApJ, 405, 538
Burstein, D., & Heiles, C. 1982, AJ, 87, 1165
Carpenter, J. M. 2001, AJ, 121, 2851
Casali, M. M., & Hawarden, T. G. 1992, JCMT-UKIRT Newsl., 4, 33
Chiosi, C., Vallenari, A., Bressan, A., Deng, L., & Ortolani, S. 1995, A&A, 293, 710
Crowl, H. H., Sarajedini, A., Piatti, A. E., Geisler, D., Bica, E., Clariá, J. J., & Santos, J. F. C. 2001, AJ, 122, 220
Da Costa, G. S., & Hatzidimitriou, D. 1998, AJ, 115, 1934
de Grijs, R., Gilmore, G. F., Johnson, R. A., & Mackey, A. D. 2002, MNRAS, 331, 245
Dirsch, B., Richtler, T., Gieren, W. P., & Hilker, M. 2000, A&A, 360, 133
Ducati, J. R., Bevilacqua, C. M., Rembold, S. B., & Ribeiro, D. 2001, ApJ, 558, 309
Elson, R. A. W. 1991, ApJS, 76, 185
Elson, R. A., & Fall, S. M. 1988, AJ, 96, 1383
Frogel, J. A., Mould, J., & Blanco, V. M. 1990, ApJ, 352, 96
Frogel, J. A., Persson, S. E., Matthews, K., & Aaronson, M. 1978, ApJ, 220, 75
Geisler, D., Bica, E., Dottori, H., Claria, J. J., Piatti, A. E., & Santos, J. F. C. 1997a, AJ, 114, 1920
Geisler, D., Bica, E., Dottori, H., Piatti, A. E., & Claria, J. J. 1997b, BAAS, 29, 841
Goudfrooij, P., Alonso, M. V., Maraston, C., & Minniti, D. 2001, MNRAS, 328, 237
Goudfrooij, P., Gilmore, D., Kissler-Patig, M., & Maraston, C. 2006, MNRAS, 369, 697
Harries, T. J., Hilditch, R. W., & Howarth, I. D. 2003, MNRAS, 339, 157
Hempel, M., & Kissler-Patig, M. 2004, A&A, 419, 863
Hill, A., & Zaritsky, D. 2006, AJ, 131, 414
Hill, V. 1999, A&A, 345, 430
Hill, V., François, P., Spite, M., Primas, F., & Spite, F. 2000, A&A, 364, L19
Hodge, P., & Flower, P. 1987, PASP, 99, 734
Hunter, D. A., Shaya, E. J., Holtzman, J. A., Light, R. M., O'Neil, E. J., & Lynds, R. 1995, ApJ, 448, 179
Jarrett, T. H., Chester, T., Cutri, R., Schneider, S., Skrutskie, M., & Huchra, J. P. 2000, AJ, 119, 2498
Jasniewicz, G., & Thevenin, F. 1994, A&A, 282, 717
Johnson, R. A., Beaulieu, S. F., Gilmore, G. F., Hurley, J., Santiago, B. X., Tanvir, N. R., & Elson, R. A. W. 2001, MNRAS, 324, 367
Kontizas, E., Dapergolas, A., Morgan, D. H., & Kontizas, M. 2001, A&A, 369, 932
Kyeong, J.-M., Tseng, M.-J., & Byun, Y.-I. 2003, A&A, 409, 479
Lançon, A., & Rocca-Volmerange, B. 1992, A&AS, 96, 593
Mackey, A. D., & Gilmore, G. F. 2003a, MNRAS, 338, 85
———. 2003b, MNRAS, 338, 120
Maraston, C. 1998, MNRAS, 300, 872
———. 2005, MNRAS, 362, 799
Maraston, C., Greggio, L., Renzini, A., Ortolani, S., Saglia, R. P., Puzia, T. H., & Kissler-Patig, M. 2003, A&A, 400, 823
Mighell, K. J., Sarajedini, A., & French, R. S. 1998, ApJ, 494, L189
Nikolaev, S., Weinberg, M. D., Skrutskie, M. F., Cutri, R. M., Wheelock, S. L., Gizis, J. E., & Howard, E. M. 2000, AJ, 120, 3340
Oliva, E., & Origlia, L. 1998, A&A, 332, 46
Olsen, K. A. G., Hodge, P. W., Mateo, M., Olszewski, E. W., Schommer, R. A., Suntzeff, N. B., & Walker, A. R. 1998, MNRAS, 300, 665
Olszewski, E. W., Schommer, R. A., Suntzeff, N. B., & Harris, H. C. 1991, AJ, 101, 515
Persson, S. E., Aaronson, M., Cohen, J. G., Frogel, J. A., & Matthews, K. 1983, ApJ, 266, 105
Persson, S. E., Murphy, D. C., Krzeminski, W., Roth, M., & Rieke, M. J. 1998, AJ, 116, 2475
Puzia, T. H., Zepf, S. E., Kissler-Patig, M., Hilker, M., Minniti, D., & Goudfrooij, P. 2002, A&A, 391, 453
Rich, R. M., Shara, M. M., & Zurek, D. 2001, AJ, 122, 842
Schlegel, D. J., Finkbeiner, D. P., & Davis, M. 1998, ApJ, 500, 525
Seggewiss, W., & Richtler, T. 1989, in Recent Developments of Magellanic Cloud Research, ed. K. S. de Boer, F. Spite, & G. Stasinska (Meudon: Obs. Paris), 45
Sirianni, M., Nota, A., Leitherer, C., De Marchi, G., & Clampin, M. 2000, ApJ, 533, 203
Skrutskie, M. F., et al. 1997, in The Impact of Large Scale Near-IR Sky Surveys, ed. F. Garzón (Dordrecht: Kluwer), 25
———. 2006, AJ, 131, 1163
Stetson, P. B. 1987, PASP, 99, 191
Suntzeff, N. B., Schommer, R. A., Olszewski, E. W., & Walker, A. R. 1992, AJ, 104, 1743
van den Bergh, S. 1981, A&AS, 46, 79
Vazdekis, A. 1999, ApJ, 513, 224
Walker, M. F. 1971, ApJ, 167, 1
Worthey, G. 1994, ApJS, 95, 107
Zaritsky, D. 1999, AJ, 118, 2824
Zaritsky, D., Harris, J., & Thompson, I. 1997, AJ, 114, 1002
Zaritsky, D., Harris, J., Thompson, I. B., & Grebel, E. K. 2004, AJ, 128, 1606
Zaritsky, D., Harris, J., Thompson, I. B., Grebel, E. K., & Massey, P. 2002, AJ, 123, 855